

Programmed Allee effect in bacteria causes a tradeoff between population spread and survival

Robert Smith^{a,1}, Cheemeng Tan^b, Jaydeep K. Srimani^a, Anand Pai^a, Katherine A. Riccione^a, Hao Song^c, and Lingchong You^{a,d,e,2}

^aDepartment of Biomedical Engineering, Duke University, Durham, NC 27708; ^bRay and Stephanie Lane Center for Computational Biology, Carnegie Mellon University, Pittsburgh, PA 15213; ^cSchool of Chemical and Biomedical Engineering, Nanyang Technological University, Singapore 637457; ^dInstitute for Genome Sciences and Policy, Duke University, Durham, NC, 27708; and ^eCenter for Systems Biology, Duke University, Durham, NC 27708

Edited by David A. Tirrell, California Institute of Technology, Pasadena, CA, and approved January 2, 2014 (received for review August 22, 2013)

Dispersal is necessary for spread into new habitats, but it has also been shown to inhibit spread. Theoretical studies have suggested that the presence of a strong Allee effect may account for these counterintuitive observations. Experimental demonstration of this notion is lacking due to the difficulty in quantitative analysis of such phenomena in a natural setting. We engineered *Escherichia coli* to exhibit a strong Allee effect and examined how the Allee effect would affect the spread of the engineered bacteria. We showed that the Allee effect led to a biphasic dependence of bacterial spread on the dispersal rate: spread is promoted for intermediate dispersal rates but inhibited at low or high dispersal rates. The shape of this dependence is contingent upon the initial density of the source population. Moreover, the Allee effect led to a tradeoff between effectiveness of population spread and survival: increasing the number of target patches during dispersal allows more effective spread, but it simultaneously increases the risk of failing to invade or of going extinct. We also observed that total population growth is transiently maximized at an intermediate number of target patches. Finally, we demonstrate that fluctuations in cell growth may contribute to the paradoxical relationship between dispersal and spread. Our results provide direct experimental evidence that the Allee effect can explain the apparently paradoxical effects of dispersal on spread and have implications for guiding the spread of cooperative organisms.

synthetic biology | quorum sensing | invasive species | cooperation | bacterial communication

A fundamental question in biology is how the spread and survival of an organism is influenced by various factors (1), including population density (2), dispersal rate (3), and habitat configuration (4). Addressing this question has implications for understanding and controlling biological invasions caused by the introduction of a new species into an established ecosystem (1), the spread of infectious diseases, or the emergence of new pathogens (5).

Dispersal has been recognized as being particularly critical in promoting successful spread (e.g., ref. 1; additional examples in *SI Text*). However, dispersal has also been shown to reduce spread (e.g., ref. 6; additional examples in *SI Text*). Theoretical studies have proposed that this paradoxical observation can be explained by the Allee effect, which is defined as a positive relationship between individual fitness and the total density of the population (7, 8). In the extreme case, called a strong Allee effect, the population will display a negative fitness, which can be manifested as a negative growth rate, when its initial density is below a critical threshold. Often, a strong Allee effect can be due to the inability to initiate a cooperative behavior at low density (7). This dynamic is observed in several contexts of biology including invasive species, reintroduction biology, epidemiology, the infection of an individual host by microbial pathogens, and quorum sensing (*SI Text*).

By assuming a strong Allee effect, theoretical studies have predicted that dispersal can have a dual effect on population survival and spread. Slow dispersal can prevent the colonization of new territories because the number of individuals arriving in

a new area is insufficient to establish a new population (e.g., ref. 9; additional examples in *SI Text*). Fast dispersal can act as a drain on a source population, which can become too small to be maintained (e.g., ref. 10; additional examples in *SI Text*). These predictions have been invoked previously to explain the failure of organisms to expand their ranges or to become established (*SI Text* and Table S1).

Although this theoretical explanation is plausible, its experimental demonstration is lacking. This is particularly difficult to verify experimentally in a natural setting because such settings are subject to numerous confounding factors that can obscure the contribution of individual components to the outcome of successful spread. Along this line, it has been suggested that environmental and demographic stochasticity may contribute to population extinction, even in species without an Allee effect (*SI Text*). The role of a strong Allee effect is further complicated by the limited number of empirical studies that demonstrate the existence of an Allee effect (11), in part due to difficulty in quantifying and studying small populations.

To overcome these difficulties, we engineered a gene circuit to confer a strong Allee effect in *Escherichia coli* and examined its impact on spread and survival. Synthetic biology involves creating novel behaviors in biological systems using gene circuits. These synthetic systems have resulted in numerous novel behaviors including spatial patterning (12) and modulation of fitness (13). Synthetic systems have several advantages over both field and theoretical studies (14). These systems provide a well-defined system to focus on the key, fundamental parameters in a more definitive manner, and they allow direct mapping between modeling

Significance

Understanding how species spread and survive is important in many biological contexts. The ability to disperse has been shown to enhance spread in some species but detract in others. Theoretical studies have predicted that these observations may be due to the Allee effect. To test this theory, we engineered *Escherichia coli* to have an Allee effect. Using these bacteria, we found that if dispersal is too fast or too slow, a population cannot spread. By manipulating the number of patches, we uncovered tradeoffs that control spread and survival. Finally, we demonstrate that fluctuations in growth may serve to determine if spread occurs. Our results may be useful in controlling invasive species and the spread of infectious diseases.

Author contributions: R.S. and L.Y. designed research; R.S., C.T., J.K.S., A.P., K.A.R., and H.S. performed research; R.S. and L.Y. contributed new reagents/analytic tools; R.S., C.T., A.P., and L.Y. analyzed data; and R.S., C.T., and L.Y. wrote the paper.

The authors declare no conflict of interest.

This article is a PNAS Direct Submission.

¹Present address: Division of Mathematics, Science and Technology, Nova Southeastern University, Fort Lauderdale, FL 33314.

²To whom correspondence should be addressed. E-mail: you@duke.edu.

This article contains supporting information online at www.pnas.org/lookup/suppl/doi:10.1073/pnas.1315954111/-DCSupplemental.

and experiments. Although modeling is often used as a driving force in such studies, the ability to confirm the model predictions in a living system serves as a critical proof-of-principle for the plausibility of these predictions. The use of synthetic gene circuits can be thought of as an extension to the use of microbes as model systems to examine questions in evolution and ecology (e.g., ref. 15).

Results

Programming a Strong Allee Effect in *E. coli*. The fundamental property of a strong Allee effect is a population that has a negative fitness level below a density threshold (*SI Text*); the population can only grow when its initial density is above a threshold density, C_{CRIT} . As such, the strong Allee effect represents a form of bistable growth (16). To realize this property, we used the LuxR/LuxI quorum-sensing (QS) system from *Vibrio fischeri* (17) and the CcdA/CcdB toxin-antitoxin module to control population survival (Fig. 1A and Fig. S1A). Induction of our circuit by isopropyl β -D-1-thiogalactopyranoside (IPTG; 1 mM) activates expression of the LuxR/LuxI system and CcdB. CcdB causes cell death by inhibiting DNA replication (18). CcdB can be inhibited by CcdA, which is controlled by the QS module. LuxI leads to synthesis of acyl-homoserine lactone (AHL). Because AHL can diffuse across the cell wall, its concentration increases with bacterial density. At a sufficiently high concentration, AHL activates LuxR, which drives the expression of CcdA. CcdA then inhibits CcdB, thus rescuing the population. Our circuit logic mimics the generation of the Allee

effect due to environmental conditioning, where a group of cooperative organisms modifies the environment to grow (Table S2).

In a natural setting, spread occurs when an organism travels from an initial area to a separate, geographically distinct area. Spread by such organisms often displays a central area of growth (i.e., source patch) surrounded by several separate areas of growth (i.e., target patch) indicative of between-patch or multipatch (i.e., multitarget or stratified) dispersal (e.g., ref. 19; additional examples in *SI Text*). These patches are often only connected by dispersal and are therefore physically separated. It has been suggested that failing to account for between-patch dispersal has led to the inability to accurately predict spread rates (20) and that an understanding of these dynamics is required to understand population spread (21).

To understand how between-patch dispersal and a strong Allee effect interact to control spread, we established a theoretical and experimental framework (*SI Text*). We initially consider two discrete patches (a source and a target patch) that are connected via one-way dispersal (from source to target). Both populations at the source and target populations are well mixed, and we do not account for any measure of distance between the patches. This two-patch system with discrete dispersal has been used extensively in the past to model the spread of species (*SI Text*). Experimentally, we emulated dispersal by discretely transferring bacteria from a source patch to a target patch and measured optical density (OD) in both patches over 28 h. Our discrete transfer protocol follows similar techniques that have been used to simulate dispersal using synthetic systems (e.g., ref. 22). Finally, our protocol may be amenable for the study of Allee effects in natural systems, including *Drosophila melanogaster* (Table S2). One could disperse an established population of flies to new medium in a separate culture and examine reproductive success.

The circuit can be modeled by two equations (Eqs. 1 and 2, *Materials and Methods*, *SI Text*, and Table S3). With the circuit OFF or ON + rescue (i.e., medium supplemented with 0.1 μ M AHL), the model predicts that the bacterial density (C) will increase regardless of initial C (Fig. S1B). With the circuit ON, the model predicts that the population will only grow when starting from a sufficiently high initial C (Fig. S1B). To test these predictions, we inoculated the engineered bacteria at varying initial densities and grew them under three conditions in a microplate reader: no IPTG (circuit OFF), 1 mM IPTG (circuit ON), and 1 mM IPTG and 0.1 μ M AHL (circuit ON + rescue). For each culture, we measured its density using OD (measured at 600 nm) every 20 min for 50 h. When the circuit was OFF or ON + rescue, the cultures grew regardless of their initial densities (Fig. S1C). When the circuit was ON, the cultures starting from a high initial density ($\sim 10^8$ cfu/mL) grew to a high density (OD = ~ 0.4) after ~ 25 h, whereas those starting from a low initial density ($\sim 10^4$ cfu/mL) did not grow over 70 h (Fig. S1C).

The OD measurements were consistent with viable cell counts measured by cfus. With the circuit OFF or ON + rescue, our model reduces to a logistic equation where the specific growth rate $[\Delta(\ln C)/\Delta t]$ is expected to decrease with initial C (Fig. 1B, blue and green lines, respectively). This was confirmed by experiment (Fig. 1C, blue and green circles/lines). When the circuit is ON, the specific growth rate is predicted to be negative for an initial C below a threshold, C_{CRIT} (Fig. 1B, red line). Above C_{CRIT} , the specific growth rate first increases and then decreases with increasing initial C , while going through a maximum at an intermediate initial C . This prediction was confirmed by experiment (Fig. 1C, red circles/lines, and Fig. S1D). When our engineered bacteria were grown with the circuit ON and from a low initial density ($< \sim 10^4$ cfu/mL), the number of cfus decreased over 28 h. Cultures starting with an initial density above $\sim 10^4$ cfu/mL grew during the same time period. The net change in culture density increased with the initial density until the latter reached

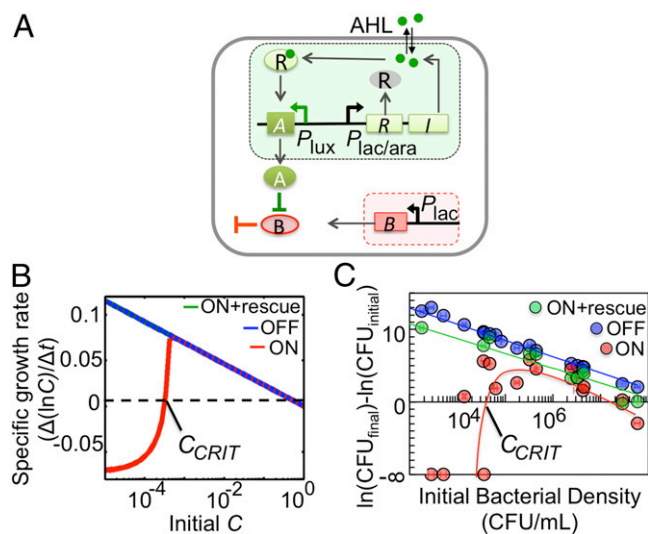


Fig. 1. Programming a strong Allee effect in *E. coli*. (A) The circuit consists of a killing module (red shaded) and a rescue module (green shaded). The killing module consists of the P_{lac} promoter driving expression of $ccdB$ (indicated by B). The rescue module consists of the $luxR(R)/luxI(I)$ quorum sensing (QS) system under the control the $P_{lac/ara}$ promoter and $ccdA$ (indicated by A) under the control of the P_{lux} promoter. Green circles, 3-oxohexanoyl-homoserine lactone (AHL). (B) Specific growth rates of the engineered bacterial population. With the circuit OFF or ON + rescue (directly behind blue line, initial rescue [A] = 0.1 μ M), the specific growth rate is predicted to decrease with increasing initial C (bacterial density). With the circuit ON, a strong Allee effect is observed; the specific growth rate is negative if the initial C is below the Allee threshold (C_{CRIT}). Specific growth rate $[\Delta(\ln C)/\Delta t]$ at $t = 100$ h. (C) Experimental verification of a strong Allee effect. With the circuit OFF (–IPTG) or ON + rescue (+IPTG/AHL), cfus decreased with increasing initial bacterial densities. With the circuit ON (+IPTG), a strong Allee effect was conferred to the population, where cfus decreased below an initial bacterial density of $\sim 10^4$ cfu/mL. Change in cfu/mL was calculated using $\ln(\text{cfu}_{\text{final}}) - \ln(\text{cfu}_{\text{initial}})$ at 28 h. When $\text{cfu}_{\text{final}}$ was 0, a result of negative infinity was obtained. SD from three replicates. Lines drawn as a guide.

$\sim 10^5$ cfu/mL. Beyond this point, the net change in culture density declined with further increases in the initial density.

C_{CRIT} is readily tunable in our system. Decreasing the degradation rate constant of AHL (k_{dA}) is predicted to increase C_{CRIT} (Fig. S24): with faster AHL degradation, a higher bacterial density is required to induce sufficient CcdA expression to rescue the population. One method to decrease AHL stability is to increase the pH of the medium (23). We observed that C_{CRIT} increased by ~ 100 -fold when our engineered bacteria were grown at pH 7.5 (compared with pH 7.0; Fig. S2 B–F). Inclusion of leaky gene expression, a metabolic burden, nonlinear activation of *ccdA*, or stochastic dynamics in our model still leads to a strong Allee effect (Fig. S2 G–J), which suggests that our simple model (Eqs. 1 and 2) is sufficient to capture the dynamics of our synthetic circuit.

A Biphasic Dependence of Population Spread on Dispersal. To guide our dispersal experiments, we modified our model (Eqs. 1 and 2) to account for the discrete transfer of bacteria from a source patch to a target patch (Eqs. S20 and S21 and Fig. S34). The modified model also accounts for death of dispersing individuals (Eq. S21 and *SI Text*) as dispersing individuals have increased rates of mortality (24). The discrete transfer of bacteria mimicked group dispersal, which has been observed in cooperative species (Table S4). Spread is assumed to have occurred when robust growth (an increase in OD greater than 0 as determined by a t test; *SI Text*) occurs at both the source and target patches (1, 25).

We first examined dispersal where only one target patch is present ($n = 1$, where n represents the number of target patches; Fig. S34). With the circuit OFF or ON + rescue, our model predicts that spread would occur for all dispersal rates (initial $C = 0.05$; Fig. 2A, *Left* and *Right*, respectively). With the circuit ON, our model predicts a biphasic dependence of the total growth (summed between the source and the target patches) on the dispersal rate (Fig. 2A, *Center*). Total growth first increases and then decreases with the dispersal rate. In the presence of a strong Allee effect, growth at either the source or the target patches increases with the initial C at the corresponding patch (after dispersal). Thus, growth at the source patch will decrease with dispersal rate (Fig. 2A, *Center*, black line) but growth at the target will increase with dispersal rate (Fig. 2A, *Center*, green line). When combined, total growth is maximized at intermediate dispersal rates, resulting in an optimal dispersal rate, which leads to the greatest amount of total growth.

To test these predictions, we emulated dispersal by transferring a fixed volume of bacteria from one well of a 96-well plate (i.e., a source well) to a second well (i.e., a target well) after an initial period of growth (*SI Text*). We chose an initial density in the source well that was above C_{CRIT} ($5.8 \pm 1.2 \times 10^6$ cfu/mL), such that bacteria would grow for all circuit states (OFF, ON, or ON + rescue) in the absence of dispersal. Our experimental system validated these predictions: with the circuit ON (Fig. 2B, *Center*, and Fig. S3 B and C), increasing dispersal rates promoted growth at the target (green line) but reduced growth at the source (i.e., dispersal rates of 0.995 and 0.975; black line), leading to a biphasic dependence of the total growth on dispersal rate (red line). An optimal dispersal rate was observed at a dispersal rate of 0.375 where the highest amount of total growth was observed. In the OFF and ON + rescue conditions, growth occurred at all dispersal rates (Fig. 2B, *Left* and *Right*). Inclusion of a death term of nondispersing individuals, the implementation of continuous dispersal, or stochastic dynamics in our model (Eqs. S22 and S23) produce the same qualitative predictions of the biphasic dependence of total growth on dispersal rate (Fig. S3 D–F and *SI Text*).

This biphasic dependence demonstrates that presence of a strong Allee effect can indeed account for the paradoxical observations on dispersal and successful spread. Our experimental

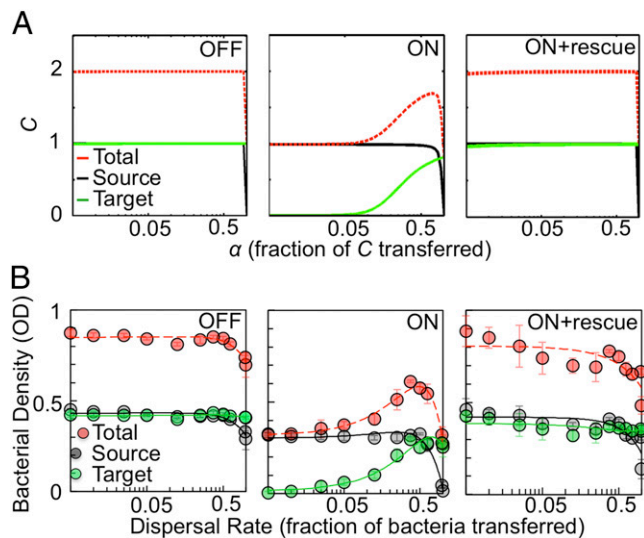


Fig. 2. A strong Allee effect causes a biphasic dependence of spread on the dispersal rate. (A) Bacterial densities (C) of a population containing our synthetic circuit with increasing α (dispersal rate). When the circuit is OFF (*Left*) or ON + rescue (initial rescue [A] = 0.1 μ M; *Right*), spread (i.e., growth at the source and target patch) is predicted to occur regardless of α . When the circuit is ON (*Center*), spread is predicted to occur within a small range of α , leading to a biphasic trend. Outside this range, growth is reduced at either the source or the target patch. Total C is the summed densities between both patches. Initial $C = 0.05$, t (simulation time) = 28 h. y axis scale is the same for each panel. (B) Density of bacterial populations containing our synthetic circuit with increasing dispersal rates. With the circuit OFF (–IPTG) or ON + rescue (+IPTG/AHL), our engineered bacteria underwent spread regardless of the dispersal rate (*Left* and *Right*, respectively). With the circuit ON (+IPTG; *Center*), our engineered bacteria had a small range of dispersal rates that led to spread. Outside this range, growth was reduced at either the target or the source patch. The lowest and highest dispersal rates that led to spread were 0.975 ($P \leq 0.04$) and 0.025 ($P \leq 0.015$, two-tailed t test; *SI Text*). SD from at least four replicates. Initial density = $5.8 \pm 1.2 \times 10^6$ cfu/mL. OD at 28 h. y axis scale is the same for each panel.

system thus provides support for two key previous theoretical predictions that have yet to be demonstrated experimentally: slow dispersal can lead to insufficient growth at the target, but fast dispersal serves as a drain at the source (*SI Text*).

Initial Source Density Determines the Range of Dispersal Rates That Allow Spread. A prominent observation in several species is that as the number of individuals released in a new area declines, so does establishment and spread success (e.g., ref. 2). Intuitively, populations with initial densities below C_{CRIT} may be more likely to go extinct. However, it remains unclear as to how the Allee effect and dispersal control spread when the initial density at the source patch increases above C_{CRIT} .

Our model predicts that with the circuit ON, increasing the initial C of the source population expands the range of dispersal rates that allow spread (Fig. 3A). At a low initial C (0.007), spread only occurs within a very small range of intermediate dispersal rates (Fig. 3B, *Left*). Here total growth is the highest at low dispersal rates where growth is reduced at the target but occurs at the source. At an intermediate initial C (0.05), a larger range of intermediate dispersal rates are predicted to promote spread (Fig. 3B, *Center*), and the total growth is the highest within this range. The range of intermediate dispersal rates that promote spread is greatly expanded for a high initial C (0.3; Fig. 3B, *Right*). In contrast, when the circuit is OFF, our model predicts that spread occurs regardless of the initial density or the dispersal rate (Fig. S3 G and H).

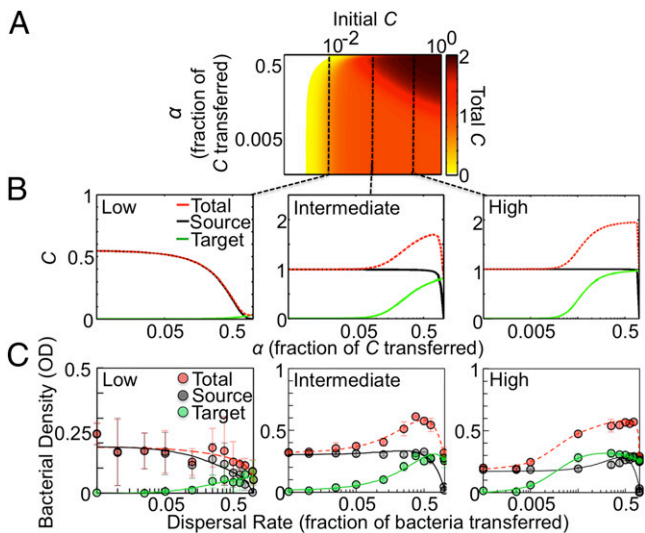


Fig. 3. Dispersal rates allowing spread depend on the initial density at the source patch. (A) Spread landscape in the presence of a strong Allee effect. Increasing the initial bacterial density (C) at the source patch expands the range of dispersal rates (α) allowing spread (i.e., growth at the source and target patches). Total C is the summed densities at the source and target patches. t (simulation time) = 28 h. (B) Slices of the spread landscape along the x axis with different initial C . Low initial $C = 0.007$, intermediate initial $C = 0.05$, and high initial $C = 0.3$. (C) Density of bacterial populations that exhibit a strong Allee effect with varying initial densities. With the circuit ON (+IPTG), increasing the initial source density by ~ 100 -fold increased the range of dispersal rates allowing spread. The highest and lowest dispersal rates that led to spread were 0.75 [$P \leq 0.005$, two-tailed t test (SI Text)] and 0.125 [$P \leq 0.043$] for low initial density, 0.975 [$P \leq 0.04$] and 0.025 [$P \leq 0.015$] for intermediate initial density, and 0.995 [$P \leq 0.006$] and 0.005 [$P < 0.001$] for high initial density. SD from six replicates. Low initial density = $6.1 \pm 1.1 \times 10^5$ cfu/mL, intermediate initial density = $5.8 \pm 1.2 \times 10^6$ cfu/mL, and high initial density = $5.5 \pm 1.4 \times 10^7$ cfu/mL. OD measured at 28 h.

Our experimental results validated these predictions (Fig. 3C). When cultures were grown with the circuit ON, spread only occurred in a small range of dispersal rates when the source well contained a low initial density of bacteria ($6.1 \pm 1.1 \times 10^5$ cfu/mL; Fig. 3C, Left). As predicted, the most amount of growth occurred at lower dispersal rates, where spread did not occur. With a 10-fold increase in the initial density (intermediate initial density, $5.8 \pm 1.2 \times 10^6$ cfu/mL; Fig. 3C, Center), intermediate dispersal rates led to spread. Here total growth is highest within the range of dispersal rates that lead to spread. The range of permissible dispersal rates was drastically expanded when the initial density at the source well was increased by another 10-fold (high initial density, $5.5 \pm 1.4 \times 10^7$ cfu/mL; Fig. 3C, Right). In contrast, with the circuit OFF, bacteria grew at both the source and the target wells regardless of the dispersal rate or the initial density of the source population (Fig. S3I).

These results suggest that species with a strong Allee effect may have two different growth patterns when arriving in a new territory with a population density slightly above C_{CRIT} . On one hand, species that disperse at a low rate will maximize their density at the source population but fail to establish a population at the target patch. On the other hand, species that disperse at a high rate may spread; however, they face the added risk of detracting from population growth should the dispersal rate not fall within the biphasic growth area. As such, although high dispersal rates would lead to successful spread when the initial density is sufficiently above C_{CRIT} , here it may serve to detract from spread success, and population growth, when the initial density is close to C_{CRIT} .

A Tradeoff Between Effectiveness of Spread and Survival. A key prediction of multitarget dispersal (in the absence of an Allee effect) is that population growth increases with increasing patches colonized making spread more prolific (20, 26). In the presence of a strong Allee effect, however, simultaneous dispersal of a small amount of bacteria to each target patch (n) may be insufficient to establish growth in the target patch but collectively can detract too much from the population at the source patch, which could lead to suppression of spread. This reasoning suggests a tradeoff between efficiency and robustness of spread and that increasing the number of target patches does not necessarily guarantee more effective total spread.

Our model predicts that with the circuit ON, the biphasic dependence of total C on dispersal rate is maintained when $n > 1$. Moreover, increasing n from 1 to 3 can increase the maximum total C for the overall population (Fig. 4A and B). However, this contracts the range of dispersal rates that allows spread, indicating a tradeoff between efficiency and robustness of spread. Our model predicts that a further increase in the number of targets ($n = 5$) not only shrinks the range of dispersal rates that allow spread but also reduces total C (Fig. 4B, Right Center). In other words, for a given dispersal rate, spread also has a biphasic dependence on n . We note that this biphasic dependence is transient because at the steady state, bacteria in all target patches would grow to carrying capacity (Fig. S4D). However, the contraction of dispersal rates allowing spread observed as n increases is still observed at steady

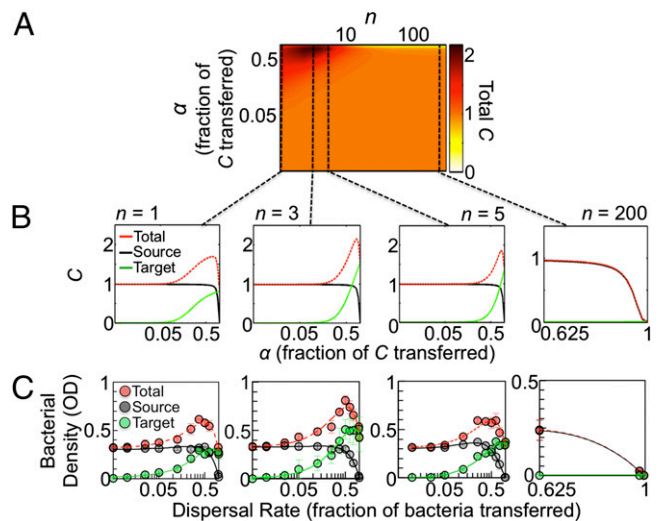


Fig. 4. A tradeoff between efficiency and robustness of spread in multitarget dispersal. (A) Spread landscape for multitarget dispersal in the presence of a strong Allee effect. Increasing n (number of target patches) can lead to an increase in the number of target patches colonized where maximum total C is highest at an intermediate n . As n increases, the range of dispersal rates allowing spread contracts. Total C is the summed densities of the source and target patches. α represents the dispersal rate. Initial $C = 0.05$, t (simulation time) = 28 h. (B) Slices of the spread landscape along the x axis with increasing values of n . (C) Density of bacterial populations with increasing dispersal rate and number of target wells. With the circuit ON (+IPTG), when the number of target wells was increased from one to three, the maximum total growth increased ($P = 0.01$; SI Text), but the range of dispersal rates allowing spread was reduced. For five target wells, the range of dispersal rates allowing spread further contracted, and total growth was reduced ($P = 0.03$). For 200 target wells, growth was observed in the source well at low dispersal rates. At high dispersal rates, growth was not observed. The highest and lowest dispersal rates that led to spread were 0.975 [$P \leq 0.04$, two-tailed t test; SI Text] and 0.025 [$P \leq 0.015$] for $n = 1$, 0.975 [$P < 0.001$] and 0.05 [$P \leq 0.008$] for $n = 3$, and 0.75 [$P \leq 0.003$] and 0.125 [$P \leq 0.003$] for $n = 5$. SD from six replicates. Experiments initiated from an initial density of $5.8 \pm 1.2 \times 10^6$ cfu/mL. OD at 28 h. See SI Text and Fig. S4 for OD calculation.

state. Furthermore, our model predicts that at $n = 200$, high dispersal rates cause complete population extinction, whereas low dispersal rates allow growth at the source patch only (Fig. 4B, *Right*). In contrast, with the circuit OFF, our model predicts the population will undergo spread regardless of the number of target patches (Fig. S4 A and B), and total C always increases with increasing n . This result is observed transiently and at the steady state (Fig. S4E).

Our experimental results validated these predictions (Fig. 4C and Fig. S4 C and F–J). Experimentally, we assumed that transfer to one target well could be used as a surrogate of transfer to multiple wells (SI Text and Fig. S4J). We transferred the same total amount of medium out of the source well but only transferred a fraction of the amount into a target well [calculated relative to the number of target wells (e.g., five target wells: 125 μL out of the source patch, 25 μL into a target patch, and the remaining 100 μL was discarded)]. We then multiplied the final bacterial density (OD) at 28 h by the total number of target wells in the system (Fig. 4C). When cultures were grown with the circuit ON and when the number of target wells was increased from one to three, the range of dispersal rates allowing spread contracted, and the maximum total growth (i.e., source well + all target wells) increased (Fig. 4C, *Left Center*). With five target wells, dispersal rates allowing spread further contracted (Fig. 4C, *Right Center*), and total growth decreased. With 200 target wells, growth was not detected in either the source or target wells at a high dispersal rate (Fig. 4C, *Right*). At low dispersal rates, growth occurred in the source well only. When the circuit was OFF, bacteria grew at all dispersal rates in both source and target wells (Fig. S4). Our analysis demonstrated that a strong Allee effect creates a tradeoff between efficient spread and survival: dispersing to multiple patches allows more efficient spread but increases the risk of failing to spread or of going extinct.

Theoretical (27) and experimental analyses (28) have demonstrated that as a population approaches a bifurcation point (e.g., C_{CRIT}), fluctuations in growth increase. Such fluctuations may serve as early indicators of catastrophic population collapse (28). Given the importance of such fluctuations toward predicting population dynamics, particularly in species with an Allee effect, we analyzed fluctuations in growth in target patches during multitarget dispersal. Our stochastic model (Eqs. S22 and S23) predicts that as α per n decreases, the distribution of $\ln C$ widens (Fig. S5A), and coefficient of variance (CV) (Fig. S5B) increases in the target patch. CV is predicted to be the lowest at dispersal rates that lead to the greatest amount of growth in the target patches. In contrast, with the circuit OFF, our stochastic model predicts that the fluctuations do not change with α per n (Fig. S5 A and B).

To test these predictions, we dispersed our engineered bacteria to one, three, or five target wells and quantified OD in the target wells. We observed that as dispersal rate per target patch increased, the distribution of $\ln\text{OD}$ widened (Fig. S5C), and CV increased (Fig. S5D) in the target patch. As predicted, CV was the lowest at dispersal rates that led to the greatest amount of growth in the target patches. In contrast, with the circuit OFF, the distribution of $\ln\text{OD}$ (Fig. S5C) and the CV (Fig. S5D) in the target well did not change significantly with dispersal rate per patch or the number of target wells. Similar trends were observed in the source well (SI Text). Our analysis indicates that fluctuations at low dispersal rates may offer an additional explanation as to why in some cases slow dispersal appears to lead to spread but in other cases it fails to result in spread.

Discussion

Our analysis has provided experimental evidence validating previous theoretical predictions that a strong Allee effect can resolve the opposite roles that dispersal has on spread success. As reflected by our results in Figs. 3 and 4, the overall outcome of

spread critically depends on several environmental factors, including the initial cell density in the source population, the presence or absence of Allee effect, the dispersal rate, the number of target sites, and the time window of the growth. Each of these factors has direct relevance to variables that are considered critical in studies of invasive species. Our modeling analysis shows that continuous dispersal (Fig. S3E) can also lead to a biphasic dependence of the population spread on the dispersal rate, suggesting that our conclusions are applicable in the absence of group dispersal. Although our experimental framework accounts for dispersal and different patches, it does not include additional aspects of the environment (e.g., environmental heterogeneity and evolution). Exclusion of these factors has allowed us to draw more definitive conclusions on the contribution of dispersal and habitat configuration to population spread.

Our results also reveal tradeoffs between spread and survival for a cooperative species exhibiting a strong Allee effect. High dispersal rates have been proposed to facilitate the spread process (e.g., ref. 29 and SI Text). However, our experimental results demonstrate that a high dispersal rate can detract from successful spread. Furthermore, we have demonstrated that the initial release size and dispersal influence spread success (Fig. 3). We observed that populations with initial densities just above C_{CRIT} maximize their total growth at low dispersal rates, where spread does not occur. Thus, fast dispersal could serve to limit population growth and may not always be favored as previously suggested. This tradeoff may explain why, during biological invasions, spread is initially slow but tends to increase over time (30). Species must achieve a minimum density in the source population before spread will occur for a particular dispersal rate. Our results may aid in guiding release sizes for reintroduced species (31) and echo previous literature that cautions against estimating the spread rate when a population is small (30).

Our results have also revealed that increasing the number of target patches presents two tradeoffs (Fig. 4). First, increasing the number of target patches decreases the range of dispersal rates that allow for spread. As such, cooperative species with an Allee effect face a tradeoff: increasing the number of target patches can result in a more prolific spread but simultaneously increases the risk of failing to spread or going extinct. Second, dispersing to an intermediate number of target patches leads to the highest population density in the short term. This result contrasts with theoretical studies that suggest that increasing the number of target patches colonized increases the total population monotonically (20). Therefore, cooperative species with a strong Allee effect follow unique spread dynamics, which may be dictated by the environment (i.e., number of target patches). This may offer an additional explanation to the highly variable spread rates observed during spread.

Our analysis has shown that as the dispersal rate per target patch decreases, fluctuations in cell growth increase (Fig. S5). This observation is in line with previous studies that have found that as a species approaches a survival threshold, an increase in fluctuations in cell growth occurs (28). Our results serve to further extend this notion to between-patch dispersal, where fluctuations may serve as an indicator of population collapse in the target patches, and may offer an additional explanation to account for the paradoxical relationship between dispersal and spread.

These results have implications for intervention programs that aim to limit control spread of a cooperative species. It has been suggested that reducing dispersal between patches can reduce or stop species from spreading (e.g., ref. 32). Intervention strategies that can reduce or prevent dispersal into different areas of the environment include a barrier zone (33), modification of the habitat to reduce dispersal (32), or the regulation of dispersal vectors (34). Our results may suggest that reduction of dispersal rate may be counterproductive, and this may push a cooperative species into a range of dispersal rates that allow optimal spread or increases

total growth. Furthermore, limiting the number of target patches to which a cooperative species is dispersing to may serve to increase the total population density.

Materials and Methods

Model Development. Our circuit can be modeled by two delayed differential equations (Eqs. 1 and 2 or Eqs. S10 and S11):

$$\frac{dC}{dt} = \mu C(1 - C) - \frac{\gamma C}{\beta + [A(t - \tau)]} \quad [1]$$

$$\frac{d[A]}{dt} = k_A C - k_{dA}[A], \quad [2]$$

where C represents the bacterial density, $[A]$ represents the concentration of AHL (μM), μ represents the maximum specific growth rate (h^{-1}), k_A represents the synthesis rate constant of AHL ($\mu\text{M h}^{-1}$), k_{dA} represents the degradation rate constant of AHL (h^{-1}), τ represents the time delay of the activation of gene expression by the LuxR–AHL complex (h), t represents simulation time (h), γ is a lumped term that represents the killing rate of CcdB ($\mu\text{M h}^{-1}$), and β is a lumped term that represents the amount of CcdA leading to half-maximal killing rate of CcdB (μM). In Eq. 1, growth is modeled by logistic kinetics, and

the AHL-mediated rescue is modeled as a Michaelis–Menten–type equation. See *SI Text* for derivation of these equations.

Strains, Growth Conditions, and Circuit Characterization. We implemented the circuit in *E. coli* strain DH5 α PRO. Single colonies were grown overnight in LB medium supplemented with chloramphenicol and kanamycin at 37 °C. Cultures were diluted in M9 medium supplemented with 2% casamino acids and 0.5% thiamine and buffered to pH 7.0 with 100 mM Mops. The circuit was induced (i.e., circuit ON) by 1 mM of IPTG. To “rescue” a population with circuit turned ON, 0.1 μM of 3-oxohexanoyl-homoserine lactone (AHL) was added. For dispersal experiments, 200- μL cultures were grown in a 96-well plate at 37 °C in a VICTOR 3 microplate reader. cfu counts were performed on LB solid medium supplemented with chloramphenicol, kanamycin, 1 mM IPTG, and 0.1 μM AHL. See *SI Text*.

ACKNOWLEDGMENTS. We thank members of the L.Y. laboratory and Dr. Naomi Cappuccino for discussion of the manuscript. This work was partially supported by the National Science Foundation (CBET-0953202), the National Institutes of Health (1R01GM098642), a DuPont Young Professorship (to L.Y.), a David and Lucile Packard Fellowship (to L.Y.), a Lane Postdoctoral Fellowship (to C.T.), and a National Science Foundation Fellowship (to K.A.R.).

- Kolar CS, Lodge DM (2001) Progress in invasion biology: Predicting invaders. *Trends Ecol Evol* 16(4):199–204.
- Hopper K, Roush R (1993) Mate finding, dispersal, number released, and the success of biological control introductions. *Ecol Entomol* 18(4):321–331.
- Elliott EC, Cornell SJ (2012) Dispersal polymorphism and the speed of biological invasions. *PLoS ONE* 7(7):e40496.
- Predick KI, Turner MG (2008) Landscape configuration and flood frequency influence invasive shrubs in floodplain forests of the Wisconsin River (USA). *J Ecol* 96(1):91–102.
- Gilligan CA, van den Bosch F (2008) Epidemiological models for invasion and persistence of pathogens. *Annu Rev Phytopathol* 46(1):385–418.
- Forsyth DM, Duncan RP, Bomford M, Moore G (2004) Climatic suitability, life-history traits, introduction effort, and the establishment and spread of introduced mammals in Australia. *Conserv Biol* 18(2):557–569.
- Allee W, Emerson A, Park O, Park T, Schmidt K (1949) *Principles of Animal Ecology* (Saunders, Philadelphia).
- Stephens PA, Sutherland WJ, Freckleton RP (1999) What is the Allee effect? *Oikos* 87(1):185–190.
- Fath G (1998) Propagation failure of traveling waves in a discrete bistable medium. *Physica D* 116(1):176–190.
- Jonsen ID, Bourchier RS, Roland J (2007) Influence of dispersal, stochasticity, and an Allee effect on the persistence of weed biocontrol introductions. *Ecol Modell* 203(3–4):521–526.
- Gregory SD, Bradshaw CJA, Brook BW, Courchamp F (2010) Limited evidence for the demographic Allee effect from numerous species across taxa. *Ecology* 91(7):2151–2161.
- Payne S, et al. (2013) Temporal control of self-organized pattern formation without morphogen gradients in bacteria. *Mol Syst Biol* 9:697.
- Nevozhay D, Adams RM, Van Itallie E, Bennett MR, Balázs G (2012) Mapping the environmental fitness landscape of a synthetic gene circuit. *PLOS Comput Biol* 8(4):e1002480.
- Tanouchi Y, Smith RP, You L (2012) Engineering microbial systems to explore ecological and evolutionary dynamics. *Curr Opin Biotechnol* 23(5):791–797.
- Chuang JS, Rivoire O, Leibler S (2009) Simpson’s paradox in a synthetic microbial system. *Science* 323(5911):272–275.
- Keitt TH, Lewis MA, Holt RD (2001) Allee effects, invasion pinning, and species’ borders. *Am Nat* 157(2):203–216.
- Miller MB, Bassler BL (2001) Quorum sensing in bacteria. *Annu Rev Microbiol* 55(1):165–199.
- Dao-Thi M-H, et al. (2005) Molecular basis of gyrase poisoning by the addiction toxin CcdB. *J Mol Biol* 348(5):1091–1102.
- Johnson DM, Liebhold AM, Tobin PC, Bjørnstad ON (2006) Allee effects and pulsed invasion by the gypsy moth. *Nature* 444(7117):361–363.
- Shigesada N, Kawasaki K, Takeda Y (1995) Modeling stratified diffusion in biological invasions. *Am Nat* 146(2):229–251.
- Hanski I (1998) Metapopulation dynamics. *Nature* 396:41–49.
- Nahum JR, Harding BN, Kerr B (2011) Evolution of restraint in a structured rock-paper-scissors community. *Proc Natl Acad Sci USA* 108(Suppl 2):10831–10838.
- You L, Cox RS, 3rd, Weiss R, Arnold FH (2004) Programmed population control by cell-cell communication and regulated killing. *Nature* 428(6985):868–871.
- Hanski I, Alho J, Moilanen A (2000) Estimating the parameters of survival and migration of individuals in metapopulations. *Ecology* 81(1):239–251.
- Lockwood JL, Cassey P, Blackburn T (2005) The role of propagule pressure in explaining species invasions. *Trends Ecol Evol* 20(5):223–228.
- Shigesada N, Kawasaki K (1997) *Biological Invasions: Theory and Practice* (Oxford University Press, Oxford).
- Dennis B (2002) Allee effects in stochastic populations. *Oikos* 96(3):389–401.
- Dai L, Vorselen D, Korolev KS, Gore J (2012) Generic indicators for loss of resilience before a tipping point leading to population collapse. *Science* 336(6085):1175–1177.
- Hill JK, Griffiths HM, Thomas CD (2011) Climate change and evolutionary adaptations at species’ range margins. *Annu Rev Entomol* 56(1):143–159.
- Taylor CM, Hastings A (2005) Allee effects in biological invasions. *Ecol Lett* 8(8):895–908.
- Dereced A, Courchamp F (2007) Importance of the Allee effect for reintroductions. *Ecoscience* 14(4):440–451.
- Brown GP, Phillips BL, Webb JK, Shine R (2006) Toad on the road: Use of roads as dispersal corridors by cane toads (*Bufo marinus*) at an invasion front in tropical Australia. *Biol Conserv* 133(1):88–94.
- Sharov AA, Liebhold AM (1998) Model of slowing the spread of gypsy moth (Lepidoptera: Lymantriidae) with a barrier zone. *Ecol Appl* 8(4):1170–1179.
- Davies KW, Sheley RL (2007) A conceptual framework for preventing the spatial dispersal of invasive plants. *Weed Sci* 55(2):178–184.

Supporting Information

Smith et al. 10.1073/pnas.1315954111

SI Materials and Methods

Strains, Growth Conditions, and Medium. *Escherichia coli* strain DH5 α PRO (Clontech) was used throughout this study unless otherwise indicated. Unless otherwise noted, experiments were performed in modified M9 medium [1X M9 salts (48 mM Na₂HPO₄, 22 mM KH₂PO₄, 862 mM NaCl, 19 mM NH₄Cl), 0.4% glucose, 2% casamino acids (Teknova), 0.5% thiamine (Calbiochem), 2 mM MgSO₄, 0.1 mM CaCl₂] buffered to pH 7.0 with 100 mM 3-(*N*-morpholino)propanesulfonic acid (Mops). We inoculated single colonies from an agar plate into 5 mL Luria–Bertani (LB) medium (Genesee Scientific). To tightly control initial conditions, overnight cultures were allowed to grow for 16 h. Short-term agar storage plates containing individual colonies were replaced every 2 wk. Unless otherwise indicated, all culture medium contained 25 μ g/mL chloramphenicol and 50 μ g/mL kanamycin. The gene circuit was activated (i.e., circuit ON condition) using 1 mM isopropyl β -D-1-thiogalactopyranoside (IPTG). Where indicated, the culture was supplemented with 0.1 μ M 3-oxohexanoyl-homoserine lactone (circuit ON + rescue, AHL; Sigma-Aldrich).

Circuit Construction (Fig. S1A). We engineered our synthetic circuit on two plasmids. To create plasmid 1 [kanamycin resistance (Kan^R), p15a origin of replication, ~20–30 copies per cell (1)], the *luxI* gene from pSND-1 (from Ron Weiss, Massachusetts Institute of Technology, Cambridge, MA) was amplified using PCR and cloned into the plasmid pLuxR (2) using the BamHI and NotI sites. The resulting plasmid contained the *P*_{lac/ara} (1) promoter driving the expression of *luxR* and *luxI* as a single transcript. To create plasmid 2 [chloramphenicol resistance (Cm^R), SC101 origin of replication, ~3–4 copies per cell (1)], the *P*_{lux} promoter and the *ccdA* gene were fused using PCR and cloned into pPROtet.E (replication origin ColE1; Clontech) using the XhoI and AatII sites. The *P*_{lac}-lacZ α -*ccdBs* (3) construct was amplified using PCR and cloned into pPROtet.E (containing *P*_{lux}-*ccdA*) using BamHI and NotI sites. Finally, the replication origin of this plasmid was replaced with SC101. This plasmid contained the *P*_{lac} promoter driving expression of a modified *ccdB* gene (lacZ α '-*ccdBs*) and the *P*_{lux} promoter driving the expression of *ccdA*. These plasmids were simultaneously transformed into *E. coli* using a Z-competent transformation kit (as per manufacturer's specifications; Zymo Research) and selected on LB agar plates containing chloramphenicol and kanamycin.

Determining the Allee Threshold (C_{CRIT}), Growth Curves, and Circuit Characterization (Fig. 1C and Fig. S1 B–D). To determine C_{CRIT} , an overnight culture was serially diluted in fresh M9 medium. Initial cfu was determined as described previously (4). Two hundred microliters of these cultures were added to a 96-well plate (REF 353219; BD Falcon). The remaining serially diluted culture was supplemented with IPTG or IPTG and AHL. Two hundred microliters of these cultures were then added to the 96-well plate. All wells were overlaid with 50 μ L of mineral oil, and the plate was placed in a microplate reader (Victor 3; Perkin-Elmer) prewarmed to 37 °C. The plate was shaken for 10 s, and optical density (OD) at 600 nm was measured every 20 min for 28 h. After 28 h, the bacterial culture was removed from the wells, and cfu was determined. Growth curves were constructed using the same protocol; however, OD was measured over 70 h, and final cfu was not measured. Background OD from cell-free medium was subtracted from each OD value.

We determined if 0.1 μ M of AHL (circuit ON + rescue) was sufficient to return the cells to their wild-type (circuit OFF)

specific growth rate. We calculated the average OD/min from 0.1 to 0.2 OD (region of exponential growth) and determined if the specific growth rates were significantly different using a two-tailed *t* test.

Modulating C_{CRIT} (Fig. S2 A–F). Our model predicts that increasing k_{dA} will increase C_{CRIT} . To test the prediction, we increased the pH of the medium from 7.0 to 7.5, which has been shown to cause faster degradation of AHL (5). We grew cells in this medium in a microplate reader as described above and determined C_{CRIT} using cfu.

To ensure that modulating the pH of the medium did not alter the growth rate, we grew cells in a microplate reader as described above in M9 medium at pH 7.0 or pH 7.5. We calculated growth rates using the differences in the natural logarithm of each OD values at 20-min interval. We then divided this value by 20 to obtain growth rate per minute. Changing the pH did not alter the growth rate because both pH conditions led to identical maximum growth rate (μ_{max}) values and similar growth rates at all time intervals.

We tested the impact of changing pH on the stability of AHL using a reporter strain. The reporter strain consisted of *E. coli* strain MG1655 containing two plasmids, one with the *P*_{lac/ara} promoter driving the expression of *luxR* (pLuxR, p15a, Kan^R) and a second with the *P*_{lux} promoter driving the expression of *gfp(uv)* [pluxGFP (uv), ColE1, Cm^R]. In addition, to examine the effect of pH on a constitutively expressed gene, we replaced pLuxR with a plasmid where *P*_{lac/ara} drives the expression of *gfp(uv)* [control strain, *P*_{lac/ara} GFP(uv), p15a, Kan^R]. We inoculated both strains from glycerol stocks into M9 medium containing kanamycin and chloramphenicol and shook them for 8 h at 37 °C. In parallel, we incubated M9 medium (buffered to pH 6.5, 7.0, or 7.5) containing 0.1 μ M AHL at 37 °C for 8 h. After 8 h, we split the medium containing AHL into two equal volumes and diluted either the reporter strain or the control strain 100 \times into the medium. Each strain was then shaken in this medium at 37 °C for 15 h. Cells were fixed with 1% formaldehyde and were analyzed by flow cytometry (BD FACSCanto II; BD Falcon). We plotted the amount of GFP fluorescence [arbitrary units (a.u.) based on FITC] from cells grown at each pH by subtracting the baseline (~280 units).

We also determined the impact that pH had on density-dependent activation of the *P*_{lux} promoter. We grew *E. coli* strain MG1655 carrying plasmid 1 (see circuit construction) and plasmid pluxGFP(uv) (see above) overnight at 30 °C in TBK medium (1% tryptone, 0.7% KCl) (6) containing kanamycin and chloramphenicol buffered to pH 7.0 with 100 mM Mops. The following day, the cells were diluted 10,000-fold into TBK medium containing 1 mM IPTG buffered to different pHs (using KOH). Note that the starting density in each of the different TBK media was the same. Two hundred microliters of each culture were then placed in a 96-well plate, overlaid with 50 μ L of mineral oil, and grown in a microplate reader at 30 °C with periodic shaking (i.e., every 10 min). Both OD and GFP(uv) fluorescence were measured every 10 min. We plotted GFP(uv) fluorescence (a.u., normalized by OD) as a function of bacterial density (OD).

Dispersal Experiments (Figs. 2 and 3 and Fig. S3 B, C, and I). An overnight culture was diluted in M9 medium. Two hundred microliters of the diluted culture (without IPTG or containing either IPTG or IPTG with AHL) were added into the odd number columns of a 96-well plate. These wells served as the surrogates of source populations. Similarly, 200 μ L of cell-free medium without IPTG, containing IPTG, or containing IPTG with AHL was

added into the even number columns of the same plate. These wells served as the surrogates of the target patches. All wells were overlaid with 50 μL of mineral oil, and the microplate was placed in a prewarmed (37 $^{\circ}\text{C}$) microplate reader. The plate was shaken for 10 s followed by an OD measurement every 20 min for 28 h. Transfer of the cells was performed at 6 h after the cells were placed in the microplate reader. Before every transfer, all wells were thoroughly resuspended. Culture was first transferred from the source to the target well. The medium was well mixed whereupon a volume of medium equal to that of the transfer volume was removed from the target well. This served to keep the total amount of medium in the target well at 200 μL . Note that removal of medium from the target well after transfer reflected the $\alpha C_{\text{target}}\delta(t_1)$ term in our equation (Eq. S21). Prewarmed medium was used to replace medium removed from the source well. The volume of this added medium was equivalent to that transferred to keep the volume of medium at the source well at 200 μL . To maintain an accurate transfer volume, when less than 0.5 μL was transferred, we diluted 1 μL of culture into fresh, prewarmed medium and transferred a volume of this diluted culture to the target or source well. We note that this small deviation in experimental procedure had no observable bearing on the results because the population in the source and target well grew to carrying capacity at low and high dispersal rates, respectively. For data analysis and presentation, background OD from cell-free medium was subtracted from each OD value. Note that we did notice some settling of the engineered bacteria (beginning at ~ 12 h for OFF and ON + rescue cultures and ~ 24 h for ON cultures). However, this is unlikely to qualitatively affect overall cell growth because AHL and nutrients diffuse quickly in liquid medium, the volume of medium (200 μL) is relatively small, and the surface area that the bacteria can settle on is relatively small.

To determine the dispersal rates that led to spread, we determined if the OD value at 28 h was significantly higher than zero using a two-tailed t test (i.e., robust growth). Spread only occurs when robust growth is observed at both the source and target patches at the same dispersal rate. We compared the dispersal rates leading to robust growth between each experimental condition to determine if the range of dispersal rates contracted or expanded. OD values below 0.01 were considered to be 0 as this is below the reading capability of our microplate reader. In the figure legends, we report the P values of the first dispersal rate that led to spread (i.e., robust growth at the source and the patch). Additional P values are not shown (i.e., for dispersal rates that did not lead to robust growth or dispersal rates where growth in the source or the target was clearly significantly different from zero).

Dispersal to Multiple Target Patches (Fig. 4 and Fig. S4 C and H–J). Multiple target patch experiments were initiated as described in *Dispersal Experiments (Figs. 2 and 3 and Fig. S3 B, C, and I)*. We assumed that the percentage of individuals leaving the source was the same and that only the number of target patches of the environment increased. As such, we transferred the same total amount of medium out of the source well but only transferred a fraction of the amount into a target well [calculated relative to the number of target wells (e.g., five targets wells: 125 μL out of the source patch, 25 μL into a target patch, and the remaining 100 μL was discarded)]. Note that we chose this approach due to the limitations of our microplate reader. Statistical significance and robust growth was determined as described in *Dispersal Experiments (Figs. 2 and 3 and Fig. S3 B, C, and I)*. In addition, we used a two-tailed t test to compare the amount of growth at the dispersal rate that led to the greatest amount of growth for $n = 1, 3, \text{ and } 5$.

We verified that one target well could function as a surrogate of n target wells (Fig. S4J). We grew cells (with IPTG) as described above and performed two types of experiments. To verify that transfer to one well could act as a surrogate for transfer to three

wells, in one experiment, we transferred equal amounts of bacterial culture to three different target wells (i.e., 25 μL or 5 μL to each of three wells) and summed the OD at 28 h of the three wells. In a second experiment, we transferred the same amount of bacterial culture to one well (i.e., 25 μL or 5 μL to one well) but multiplied the OD value at 28 h by 3. We then compared the summed OD values at 28 h produced by these two methods to determine if one target well could function as a surrogate of n target wells. We also repeated the above experiment to ensure that one well could act as a surrogate of five wells by using five wells (experiment 1) or by multiplying by five (experiment 2). We note that verification of $n = 200$ was beyond the capability of our microplate reader.

Stochasticity and Multiple Target Patches (Fig. S5 C and D). To analyze fluctuations in cell growth in the target well, we used OD in target wells at 28 h. We plotted $\ln\text{OD}$ of each target well and the coefficient of variance (CV) as a function of dispersal rate per target patch. Alternatively to the protocol described above [*Dispersal to Multiple Target Patches (Fig. 4 and Fig. S4 C and H–J)*], we dispersed cells to the actual number of target patches (i.e., when $n = 3$, we transferred cells to three different wells of a 96-well plate) but kept the overall experimental protocol identical. After 28 h, we measured the OD in each of the target wells. We plotted $\ln\text{OD}$ of each target well and CV. We note that analysis of the $\ln\text{OD}$ and CV in the source patch yielded qualitatively similar trends. The removal of background fluctuations by the microplate reader does not change our results qualitatively.

SI Results

Cooperation Can Lead to a Strong Allee Effect. A fundamental property for the strong Allee effect is negative fitness (e.g., growth) below a critical population density. Here the population grows only when starting from a density higher than the critical population density. This property is observed in several contexts throughout biology and is particularly relevant to cooperating organisms. Several specific examples of these cooperative organisms are summarized in Table S2.

The Allee effect is most often studied within the context of studying terrestrial or aquatic animals. Specifically, the Allee effect has been observed in noninvasive (7), invasive (8), and endangered/reintroduced species (9). Although there are several mechanisms (i.e., predation and inability to find mates) (10) that can result in Allee effect in these contexts, several of these involve cooperation, including cooperative breeding (11), cooperative defense (12), cooperative feeding (13), and cooperative temperature regulation (14).

A strong Allee effect also is prevalent in infectious disease. The concept of a minimal infective dose, whereby a pathogen cannot infect a host if the pathogen is below a critical density, is well established (15–17). It has been hypothesized that in some cases, a minimal infective dose is required for the infectious agent to cooperate and release sufficient quantities of diffusible molecule to overwhelm the immune system (15). Similarly, several pathogens cannot activate virulence factors below a critical population threshold and are thus prone to clearing by the immune system (18, 19). Many pathogens form antibiotic-resistant biofilms (20–22) and can be regulated through density-dependent quorum sensing signals (23). Finally, an Allee effect is also observed in the inoculum effect, where a given density of bacteria cooperates to grow in the presence of an antibiotic (24, 25).

Although not commonly referred to as a strong Allee effect in epidemiology, several models have assumed this property. In these models, for a given range of basic reproduction ratio values (R_0), the factor that determines whether a disease successfully spreads within a population is determined by the initial number of infected individuals or pathogens introduced into a population of susceptible individuals (26). Nonconstant transmission rates

that produce this bistability have been used in susceptible-infected-removed (SIR) (27) and susceptible-infected-susceptible (SIS) (28, 29) models. Although these models do not necessarily account for cooperation between infected individuals explicitly, they are nevertheless relevant in the context of our manuscript (i.e., Allee effect and dispersal).

Defining the Allee Effect. In our study, we have adopted the textbook definition of Allee effect: the overall fitness (or one of its components) is positively related to population size or density (10, 30–32). We chose this definition because it appears to be the most consistent definition in the literature, although many additional definitions of the Allee effect have been proposed (reviewed in ref. 10). We note that this definition, or very similar definitions, is applicable (and has been applied previously) to both well-mixed systems, both nonspatial (e.g., ref. 33) and spatial (e.g., refs. 34 and 35), and nonmixed spatial systems (e.g., ref. 36). Alternative definitions for the Allee effect include inverse density dependence (37), dispensatory dynamics (or depensation) (38), and sigmoidal dose dependence (16). Additional definitions, including strong and weak Allee effects and demographic and component Allee effects, are formally reviewed elsewhere (10, 31).

Theoretical Studies Examining Dispersal, Spread, and the Allee Effect. The paradoxical relationship between dispersal and spread success is founded and observed from many studies in the literature. On one hand, several studies have shown that high dispersal promotes successful spread (39–44). We note that several studies have also demonstrated that high dispersal is often favored (or selected for) during a biological invasion (45–47). On the other hand, several studies have also found dispersal to be negatively associated with successful spread (48–51). In some studies, as outlined below, the Allee effect has been used to explain these conflicting trends.

Several previous studies have used spatial models to examine how the Allee effect and dispersal interact during the spread process. Most pertinent to our study are those that demonstrate that insufficient dispersal will not allow an established colony to spread and that sufficiently fast dispersal can act as a drain on an established population. In support of the former, Keitt et al. developed a spatially discrete ordinary differential equation model (with patchy landscapes) to show that insufficient dispersal can prevent spread into new areas (52). Similarly, Hadjiavougosti and Ichtiaroglou used a heuristic, discrete space–time model consisting of a one-dimensional chain of identical sites to demonstrate a similar phenomenon (53). Finally, Veit and Lewis (54) used a reaction–diffusion model to offer an explanation for the slow spread of introduced house finches. Here they postulated that insufficient dispersal and the Allee effect inhibited the spread rate during the initial stages of the invasion. In support of the latter, South and Kenward used a stochastic, individual-based, spatially continuous model consisting of a grid of homogenous hexagonal cells to examine how dispersal distance and mate-finding abilities affects spread (55). They observed that high dispersal distance (and low mate finding) could result in population decline (and thus no spread). Robinet et al. used a homogenous spatially explicit individual-based lattice model to examine the effect of dispersal on mating and survival (56). They observed that as temporal or spatial dispersal was increased, a reduction in mating success, and thus proliferation of the established colony, was observed. In a follow-up study, Robinet and Liebhold used a spatially explicit, stochastic individual-based model where the exact location of each individual was mapped in a continuous space that did not contain boundaries (36). Using this model, they observed that as dispersal increased, growth rates and the probability of establishment declined significantly.

Dispersal to Target Patches in the Environment. Several species (e.g., refs. 57–60), including those with a strong Allee effect (61), have been observed to colonize multiple target patches outside of a single heavily colonized area. It has been postulated that this dispersal may result from spatial heterogeneity in the environment (e.g., ref. 62). Spatial heterogeneity arises from an environment where there is a discontinuous distribution of patches that are suitable for colonization (e.g., ref. 63). As such, continuous spread from the source patch to all patches is not possible. This leads to multiple, isolated target patches becoming colonized outside of the source patch. Furthermore, stratified dispersal (e.g., refs. 59, 64, and 65) may also allow the colonization of multiple areas outside of a central area of growth (i.e., source). Here growth outside the source does not occur in discrete patches but occurs in a homogeneous environment where individual colonies can grow and coalesce with each other.

Our experimental system was designed to mimic this critical aspect of the spread process, mainly to show that dispersal can occur to separate distinct areas of the environment that sit outside of the central area of growth (i.e., source patch). To accomplish this, our theoretical system consists of two patches: a source patch, where a population of organisms initially resides, and a target patch, where the population at the source patch can disperse. The bacteria in each of the patches are well mixed, and we do not consider any measure of distance between the patches. Although the aforementioned studies (*Theoretical Studies Examining Dispersal, Spread, and the Allee Effect*) use multiple modeling frameworks to examine spread (i.e., spatially continuous homogenous systems and patchy systems), the use of a two-patch system is a well-established method to study dispersal (66, 67), as well as dispersal for species with an Allee effect (28, 34, 68). Using this theoretical approach allowed us to connect our theoretical system to our experimental systems. Furthermore, due to its relative simplicity, we could draw conclusions without taking into account multiple interacting factors of spatial spread observed in other theoretical models (e.g., distance, spread rate, and stochasticity).

Model Development (Fig. 1B and Fig. S1B). We model the synthetic bacterial population using five delayed differential equations:

$$\frac{dC}{dt} = \mu C(1 - C) - \frac{k_{kill}[CcdB]}{K + [CcdB]} C \quad [S1]$$

$$\frac{d[A]}{dt} = k_A C - k_{dA}[A] \quad [S2]$$

$$\begin{aligned} \frac{d[CcdA]}{dt} = & k_{ca}[A(t - \tau)] - k_{d1}[CcdA] - k_f[CcdA].[CcdB] \\ & + k_b[CcdA - CcdB] \end{aligned} \quad [S3]$$

$$\frac{d[CcdB]}{dt} = k_I - k_{d2}[CcdB] - k_f[CcdA].[CcdB] + k_b[CcdA - CcdB] \quad [S4]$$

$$\begin{aligned} \frac{d[CcdA - CcdB]}{dt} = & k_f[CcdA].[CcdB] - k_b[CcdA - CcdB] \\ & - k_{d3}[CcdA - CcdB] \end{aligned} \quad [S5]$$

where C represents the bacterial density normalized with respect to the carrying capacity and is unitless, $[A]$ represents the concentration of AHL (μM), $[CcdA]$ represents the concentration of CcdA (antidote) (μM), $[CcdB]$ represents the concentration of CcdB (toxin) (μM), $[CcdA - CcdB]$ represents the concentration of the CcdA–CcdB complex (μM), μ represents the maximum

specific growth rate (h^{-1}), K represents the CcdB concentration that gives rise to the half maximal killing rate (μM), k_{kill} represents the bacterial killing rate by CcdB (h^{-1}), k_A represents the synthesis rate constant of AHL ($\mu M h^{-1}$), k_{dA} represents the degradation rate constant of AHL (h^{-1}), k_{ca} represents the expression rate constant of CcdA (h^{-1}), τ represents the time delay of the activation of gene expression by the LuxR–AHL complex (h), t represents time (h), k_{d1} represents the degradation rate constant of CcdA (h^{-1}), k_f represents the association rate constant of CcdA to CcdB (h^{-1}), k_b represents the dissociation rate constant of CcdA–CcdB complex ($\mu M^{-1} h^{-1}$), k_I represents the synthesis rate constant of CcdB ($\mu M h^{-1}$), k_{d2} represents the degradation rate constant of CcdB (h^{-1}), and k_{d3} represents the degradation rate constant of CcdA–CcdB complex (h^{-1}).

In this model, we assume that AHL diffusion is much faster than gene expression or growth kinetics, such that the concentrations of the intracellular AHL and extracellular AHL are equal (69). As a result, the synthesis rate of AHL is linearly dependent on C [the first right-hand-side (RHS) term of Eq. S2]. Our circuit would only be activated by intracellular AHL because the LuxR receptor is an intracellular receptor (70). We assume that the synthesis rate of CcdA is linearly dependent on AHL concentration with a time delay due to circuit activation (Eq. S10 and the first RHS term of Eq. S3) and that the synthesis rate of CcdB is constant (controlled directly by IPTG) (the first RHS term of Eq. S4). Production rates are given per cell, with the exception of AHL.

Assuming the CcdA–CcdB complex, CcdA, and CcdB to be at quasi-steady state, we obtained Eqs. S6–S8 (from Eqs. S3–S5):

$$[CcdA - CcdB] = \frac{k_f [CcdA] \cdot [CcdB]}{k_b + k_{d3}} \quad [S6]$$

$$[CcdA] \approx \frac{k_{ca} [A(t-\tau)]}{k_{d3} k_f [CcdB]} \quad [S7]$$

$$[CcdB] \approx \frac{k_I - k_{ca} [A(t-\tau)]}{k_{d2}} \quad [S8]$$

In the solution of Eq. S7, we have simplified the equation by taking into account that the degradation rate of CcdA is faster than that of CcdB (71), the dissociation constant of CcdA–CcdB complex is ~ 0.032 nM (72), and the concentration of CcdB is greater than 10 molecules per bacterium (10 nM) due to promoter activation by IPTG (1). These simplifying assumptions can be relaxed, which will lead to a different (more complex) form of the final equations. However, these alternative equations would generate qualitatively the same predictions (e.g., generation of Allee effect when the circuit is induced; not shown).

We substitute Eq. S8 into Eq. S1 and obtain Eq. S9:

$$\frac{dC}{dt} = \mu C(1-C) - \frac{\gamma C}{\beta + [A(t-\tau)]}, \quad [S9]$$

where $\gamma = \frac{k_{kill} k_f^2}{k_{d2} k_{ca} K}$ ($\mu M h^{-1}$) and $\beta = \frac{k_I}{k_{ca}} \left(1 + \frac{k_f}{K k_{d2}}\right)$ (μM). To estimate the magnitude of the lumped parameters, we first estimated several parameters based on literature data (Table S3). We used these parameters to estimate the magnitude of the lumped parameters γ and β . To estimate k_I , we used previously reported values of transcription (73) and translation rates (74), cell volume [$\sim 4 \times 10^{-15}$ L (75)], the time required for protein folding (~ 10 s per protein, estimated), and the molecular weight of our modified CcdB (~ 21.36 kDa). We estimated that γ would have a magnitude of $0.001 \mu M h^{-1}$ and β would have a magnitude of $0.001 \mu M$.

Therefore, Eqs. S1–S5 can be simplified to the following two delayed differential equations:

$$\frac{dC}{dt} = \mu C(1-C) - \frac{\gamma C}{\beta + [A(t-\tau)]} \quad [S10]$$

$$\frac{d[A]}{dt} = k_A C - k_{dA} [A]. \quad [S11]$$

Previous studies have reported the induction threshold of the LuxR/3-oxohexanoyl-homoserine lactone (3OC6HSL) system at ~ 0.005 – $0.010 \mu M$ and maximal induction at $\sim 0.7 \mu M$ of DL-3OC6HSL (76). However, $0.1 \mu M$ of DL-3OC6HSL (76) leads to near maximal induction of the *luxR* system and was therefore selected as the quantity of AHL to add to experimental analyses for control experiments. Finally, LuxR–AHL complex reaches quasi steady states quickly (77) and therefore was not explicitly accounted for in our set of equations.

To obtain parameters for Eqs. S10 and S11, we estimated μ by using the growth data presented in Fig. S1C. τ was first estimated by examining the time point (h) at which growth was detected in induced cultures (i.e., growth with IPTG) in the microplate reader (Fig. S1C). We took this value and divided it by half to account for the time required to synthesize *ccdA*, for *ccdA* to bind to *ccdB*, and for cells to recover. Previous studies have found that rescue after poisoning with *ccdB* causes cells to have a recovery time (78). The order of magnitude of β and γ were estimated as described above. We then fit the values of β and γ to our experimental data. Parameters of the simplified model are presented in Table S3.

Leaky Expression of AHL (Fig. S2G). To examine the impact of leaky expression of AHL on system dynamics, we modified Eqs. S10 and S11 to Eqs. S12 and S13:

$$\frac{dC}{dt} = \mu C(1-C) - \frac{\gamma C}{\beta + [A(t-\tau)]} \quad [S12]$$

$$\frac{d[A]}{dt} = k_{leaky} + k_A C - k_{dA} [A], \quad [S13]$$

where k_{leaky} represents the leaky expression of AHL ($\mu M h^{-1}$). Inclusion of a small basal (or leaky) expression term of AHL synthesis in our model does not affect the qualitative predictions of the model (Fig. S2G). However, for a large basal expression value, a strong Allee effect is not observed, which thus conflicts with results presented in Figs. 1C and 2B. Previous studies using the promoters implemented in our synthetic circuit have observed nearly undetectable expression when the promoter remains uninduced (1). Although we did not explicitly check for leaky expression in our experimental system (i.e., the concentration of AHL in uninduced cultures), the leaky expression is likely $< 10^{-4} \mu M h^{-1}$ and appears to not fundamentally influence our experimental results.

Metabolic Burden of AHL Expression (Fig. S2H). To examine the impact of metabolic burden of AHL expression on system dynamics, we modified Eqs. S10 and S11 to Eqs. S14 and S15:

$$\frac{dC}{dt} = \frac{\mu}{1 + [A]/k_{met}} C(1-C) - \frac{\gamma C}{\beta + [A(t-\tau)]} \quad [S14]$$

$$\frac{d[A]}{dt} = k_A C - k_{dA} [A], \quad [S15]$$

where k_{met} represents the scaling constant of specific growth rates μ with respect to the amount of AHL (μM). A low k_{met} value would give rise to a strong metabolic burden of AHL

expression. Inclusion of the metabolic burden associated with the expression of AHL increases the amount of time required to reach steady state but does not qualitatively alter our results (Fig. S2H). A sufficiently large metabolic burden (Fig. S2H, brown line) does not allow cell growth to occur.

Nonlinear Activation of AHL Expression (Fig. S2J). To examine the impact of nonlinear *CcdA* synthesis on system dynamics, we modified Eqs. S10 and S11 to Eqs. S16 and S17:

$$\frac{dC}{dt} = \mu C(1 - C) - \frac{\gamma C}{\beta + \frac{[A(t - \tau)]^2}{K_{AHL}^2 + [A(t - \tau)]^2}} \quad [\text{S16}]$$

$$\frac{d[A]}{dt} = k_A C - k_{dA} [A], \quad [\text{S17}]$$

where K_{AHL} represents the half maximal constant of AHL-mediated gene expression (μM). We note that this alternative model that considered the activation of the *ccdA* gene via a LuxR–AHL dimer complex (modeled as a Hill's function) produced qualitatively the same results. We used a cooperativity value of 2, which is slightly larger than the values (0.85–1.6) reported previously (79, 80).

Stochastic Model of Allee Effect (Fig. S2J). Although our model (Eqs. S10 and S11) is deterministic, stochastic models (accounting for stochastic environmental components or demographic components) have also been used to study the Allee effect. To examine the influence of stochasticity in our model, we modified Eqs. S10 and S11 to Eqs. S18 and S19:

$$dC = \left(\mu C(1 - C) - \frac{\gamma C}{\beta + A(t - \tau)} \right) dt + N_1(0, \sigma) \sqrt{\left| \mu C(1 - C) - \frac{\gamma C}{\beta + A(t - \tau)} \right|} \sqrt{dt} \quad [\text{S18}]$$

$$d[A] = (k_A C - k_{dA} [A]) dt + N_2(0, \sigma) \sqrt{|k_A C - k_{dA} [A]|} \sqrt{dt}, \quad [\text{S19}]$$

where $N(0, \sigma)$ represents white noise with SD σ . In the stochastic model containing an Allee effect, C_{CRIT} becomes probabilistic, which has a dual effect on establishment: it can increase the likelihood of population extinction when the population is above C_{CRIT} and can increase the likelihood of population establishment when the population is below C_{CRIT} . This observation is consistent with a previous theoretical study (81). Stochasticity in models of population establishment without an Allee effect can also result in extinction of small populations due to demographic stochasticity (81); however, this is often not considered to be a true Allee effect. We did not perform statistical analysis for robust growth using the stochastic equations.

Modeling Between-Patch Dispersal (Figs. 2A, 3A and B, and 4A and B and Figs. S3D, E, G, and H; S4A, B, and D–G). To model the between-patch dispersal, we extend our base model (Eqs. S10 and S11) by including a discrete dispersal parameter (δ) to model the transfer of a fraction of bacteria (α , dispersal rate) from the source patch to the target patch and a death term to account for death or loss of bacteria during transfer:

$$\frac{dC_{\text{source}}}{dt} = -\alpha C_{\text{source}} \delta(t_1) + \mu C_{\text{source}} (1 - C_{\text{source}}) - \frac{\gamma C_{\text{source}}}{\beta + [A(t - \tau)]_{\text{source}}} \quad [\text{S20}]$$

$$\frac{dC_{\text{target}}}{dt} = \alpha C_{\text{source}} \delta(t_1) + \mu C_{\text{target}} (1 - C_{\text{target}}) - \frac{\gamma C_{\text{target}}}{\beta + [A(t - \tau)]_{\text{target}}} - \alpha C_{\text{target}} \delta(t_1), \quad [\text{S21}]$$

where $\delta(t_1)$ is a dirac delta function with $t_1 = kT_0$ and T_0 represents the period of transfer. C_{source} and C_{target} represent the bacterial density at either the source or the target patches. In both cases, bacterial density is normalized to the carrying capacity and is unitless.

The first RHS terms in both Eqs. S20 and S21 represent the discrete dispersal of a bacterial population. We note that α may not constitute the true definition of a rate; however, the term “dispersal rate” has been used to describe both continuous and discrete (e.g., ref. 82) dispersal in the literature. The inclusion of the death term (the fourth RHS term) in Eq. S21 represents the increased mortality observed during dispersal events (83–85). Exclusion of the term from our model continues to produce a biphasic relationship between dispersal and spread, as does the inclusion of a death term for individuals at the source (i.e., those that do not disperse; Fig. S3D). If dispersal is modeled as a continuous function, the model continues to predict a biphasic relationship between dispersal rate and spread (Fig. S3E). In the implementation of our model, we also account for the transfer of AHL between the wells but do not account specifically for the memory of the LuxR–AHL complex. Previous studies have indicated that the LuxR–AHL complex is unstable once the concentration of AHL drops below the activation threshold (77).

Several studies have indicated that between-patch dispersal can occur via long-distance dispersal, which is most often mediated by nonnatural means, such as human transport (57). Although our model can be used to describe this type of dispersal, our model does not explicitly assume any measure of distance but simply assumes that growth, and the accumulation of AHL, is independent in both populations (i.e., source and target populations).

Modeling Stochasticity in Between-Patch Dispersal (Figs. S3F and S5A and B). To examine the influence of stochasticity in our dispersal model, we modified Eqs. S20 and S21 to Eqs. S22 and S23:

$$dC_{\text{source}} = \left(-\alpha C_{\text{source}} \delta(t_1) + \mu C_{\text{source}} (1 - C_{\text{source}}) - \frac{\gamma C_{\text{source}}}{\beta + [A(t - \tau)]_{\text{source}}} \right) dt + N_1(0, \sigma) \sqrt{dt} \quad [\text{S22}]$$

$$dC_{\text{target}} = \left(\alpha C_{\text{source}} \delta(t_1) + \mu C_{\text{target}} (1 - C_{\text{target}}) - \frac{\gamma C_{\text{target}}}{\beta + [A(t - \tau)]_{\text{target}}} - \alpha C_{\text{target}} \delta(t_1) \right) dt + N_2(0, \sigma) \sqrt{dt}, \quad [\text{S23}]$$

where $N(0, \sigma)$ represents white noise with SD σ . Implementation of this model continues to predict a biphasic relationship between dispersal rate and spread.

To examine fluctuations in C in the target patch, we used noise of SDE of 0.01 and noise of transfer of 0.1. Initial C was 0.5, and $t = 28$ h.

- Lutz R, Bujard H (1997) Independent and tight regulation of transcriptional units in *Escherichia coli* via the LacR/O, the TetR/O and AraC/1-2 regulatory elements. *Nucleic Acids Res* 25(6):1203–1210.
- Collins CH, Arnold FH, Leadbetter JR (2005) Directed evolution of *Vibrio fischeri* LuxR for increased sensitivity to a broad spectrum of acyl-homoserine lactones. *Mol Microbiol* 55(3):712–723.
- Balagaddé FK, et al. (2008) A synthetic *Escherichia coli* predator-prey ecosystem. *Mol Syst Biol* 4:187.
- Kohanski MA, Dwyer DJ, Hayete B, Lawrence CA, Collins JJ (2007) A common mechanism of cellular death induced by bactericidal antibiotics. *Cell* 130(5):797–810.
- You L, Cox RS, 3rd, Weiss R, Arnold FH (2004) Programmed population control by cell-cell communication and regulated killing. *Nature* 428(6985):868–871.
- Pai A, Tanouchi Y, You L (2012) Optimality and robustness in quorum sensing (QS)-mediated regulation of a costly public good enzyme. *Proc Natl Acad Sci USA* 109(48):19810–19815.
- Wells H, Strauss EG, Rutter MA, Wells PH (1998) Mate location, population growth and species extinction. *Biol Conserv* 86(3):317–324.
- Cappucino N (2004) Allee effect in an invasive plant, pale swallow wort *Vincetoxicum rossicum* (Asclepiadaceae). *Oikos* 106(1):3–8.
- Treydte AC, et al. (2001) In search of the optimal management strategy for Arabian oryx. *Anim Conserv* 4(3):239–249.
- Courchamp F, Berec L, Gascoigne J (2008) *Allee Effects in Ecology and Conservation* (Oxford University Press, Oxford).
- Brown CR, Brown MB (2004) Group size and ectoparasitism affect daily survival probability in a colonial bird. *Behav Ecol Sociobiol* 56(5):498–511.
- Clutton-Brock TH, et al. (1999) Predation, group size and mortality in a cooperative mongoose, *Suricata suricatta*. *J Anim Ecol* 68(4):672–683.
- Tobin PC, Berec L, Liebhold AM (2011) Exploiting Allee effects for managing biological invasions. *Ecol Lett* 14(6):615–624.
- Stephens PA, Frey-Roos F, Arnold W, Sutherland WJ (2002) Model complexity and population predictions. The alpine marmot as a case study. *J Anim Ecol* 71(2):343–361.
- Schmid-Hempel P, Frank SA (2007) Pathogenesis, virulence, and infective dose. *PLoS Pathog* 3(10):1372–1373.
- Regoes RR, Ebert D, Bonhoeffer S (2002) Dose-dependent infection rates of parasites produce the Allee effect in epidemiology. *Proc Biol Sci* 269(1488):271–279.
- Ebert D, Rohringer Z, Carius HJ (2000) Dose effects and density-dependent regulation of two microparasites of *Daphnia magna*. *Oecologia* 122(2):200–209.
- Ji G, Beavis RC, Novick RP (1995) Cell density control of staphylococcal virulence mediated by an octapeptide pheromone. *Proc Natl Acad Sci USA* 92(26):12055–12059.
- Antunes LCM, Ferreira RBR, Buckner MMC, Finlay BB (2010) Quorum sensing in bacterial virulence. *Microbiology* 156(Pt 8):2271–2282.
- Stewart PS, Costerton JW (2001) Antibiotic resistance of bacteria in biofilms. *Lancet* 358(9276):135–138.
- Mah T-FC, O'Toole GA (2001) Mechanisms of biofilm resistance to antimicrobial agents. *Trends Microbiol* 9(1):34–39.
- Mah T-F, et al. (2003) A genetic basis for *Pseudomonas aeruginosa* biofilm antibiotic resistance. *Nature* 426(6964):306–310.
- Shih P-C, Huang C-T (2002) Effects of quorum-sensing deficiency on *Pseudomonas aeruginosa* biofilm formation and antibiotic resistance. *J Antimicrob Chemother* 49(2):309–314.
- Brook I (1989) Inoculum effect. *Rev Infect Dis* 11(3):361–368.
- Tan C, et al. (2012) The inoculum effect and band-pass bacterial response to periodic antibiotic treatment. *Mol Syst Biol* 8:617.
- Gilligan CA, van den Bosch F (2008) Epidemiological models for invasion and persistence of pathogens. *Annu Rev Phytopathol* 46(1):385–418.
- Liu WM, Levin SA, Iwasa Y (1986) Influence of nonlinear incidence rates upon the behavior of SIRs epidemiological models. *J Math Biol* 23(2):187–204.
- Castillo-Chavez C, Yakubu A-A (2001) Dispersal, disease and life-history evolution. *Math Biosci* 173(1):35–53.
- van den Driessche P, Watmough J (2000) A simple SIS epidemic model with a backward bifurcation. *J Math Biol* 40(6):525–540.
- Allee W, Emerson A, Park O, Park T, Schmidt K (1949) *Principles of Animal Ecology* (Saunders, Philadelphia).
- Stephens PA, Sutherland WJ, Freckleton RP (1999) What is the Allee effect? *Oikos* 87(1):185–190.
- Taylor CM, Hastings A (2005) Allee effects in biological invasions. *Ecol Lett* 8(8):895–908.
- Berec L, Angulo E, Courchamp F (2007) Multiple Allee effects and population management. *Trends Ecol Evol* 22(4):185–191.
- Gyllenberg M, Hemminki J, Tammaru T (1999) Allee effects can both conserve and create spatial heterogeneity in population densities. *Theor Popul Biol* 56(3):231–242.
- Amarasekare P (1998) Interactions between local dynamics and dispersal: Insights from single species models. *Theor Popul Biol* 53(1):44–59.
- Robinet C, Liebhold AM (2009) Dispersal polymorphism in an invasive forest pest affects its ability to establish. *Ecol Appl* 19(7):1935–1943.
- Courchamp F, Clutton-Brock T, Grenfell B (1999) Inverse density dependence and the Allee effect. *Trends Ecol Evol* 14(10):405–410.
- Rowe S, Hutchings JA, Bekkevold D, Rakin A (2004) Depensation, probability of fertilization, and the mating system of Atlantic cod (*Gadus morhua* L.). *ICES J Mar Sci* 61(7):1144–1150.
- Davis MA (2009) *Invasion Biology* (Oxford University Press, Oxford).
- Kolar CS, Lodge DM (2001) Progress in invasion biology: predicting invaders. *Trends Ecol Evol* 16(4):199–204.
- Rejmanek M, Richardson DM (1996) What attributes make some plant species more invasive? *Ecology* 77(6):1655–1661.
- Ehrlich PR (1989) Attributes of invaders and the invading processes: Vertebrates. *Biological Invasions: A Global Perspective*, eds Drake JA, et al. (John Wiley, Chichester), pp 315–328.
- Lockwood JL, Cassey P, Blackburn T (2005) The role of propagule pressure in explaining species invasions. *Trends Ecol Evol* 20(5):223–228.
- Bubb DH, Thom TJ, Lucas MC (2006) Movement, dispersal and refuge use of co-occurring introduced and native crayfish. *Freshw Biol* 51(7):1359–1368.
- Hill JK, Griffiths HM, Thomas CD (2011) Climate change and evolutionary adaptations at species' range margins. *Annu Rev Entomol* 56(1):143–159.
- Travis J, Dytham C (2002) Dispersal evolution during invasions. *Evol Ecol Res* 4:1119–1129.
- Phillips BL, Brown GP, Shine R (2010) Evolutionarily accelerated invasions: The rate of dispersal evolves upwards during the range advance of cane toads. *J Evol Biol* 23(12):2595–2601.
- Forsyth DM, Duncan RP, Bomford M, Moore G (2004) Climatic suitability, life-history traits, introduction effort, and the establishment and spread of introduced mammals in Australia. *Conserv Biol* 18(2):557–569.
- Veltman CJ, Nee S, Crawley MJ (1996) Correlates of introduction success in exotic New Zealand birds. *Am Nat* 147(4):542–557.
- Duncan RP, Blackburn TM, Sol D (2003) The ecology of bird introductions. *Annu Rev Ecol Syst* 34(1):71–98.
- Cassey P (2002) Life history and ecology influences establishment success of introduced land birds. *Biol J Linn Soc* 76(4):465–480.
- Keitt TH, Lewis MA, Holt RD (2001) Allee effects, invasion pinning, and species' borders. *Am Nat* 157(2):203–216.
- Hadjiagousti D, Ichtarioglou S (2004) Existence of stable localized structures in population dynamics through the Allee effect. *Chaos Solitons Fractals* 21(1):119–131.
- Veit RR, Lewis MA (1996) Dispersal, population growth, and the Allee effect: Dynamics of the house finch invasion of eastern North America. *Am Nat* 148(2):255–274.
- South AB, Kenward RE (2001) Mate finding, dispersal distances and population growth in invading species: A spatially explicit model. *Oikos* 95(1):53–58.
- Robinet C, et al. (2008) Dispersion in time and space affect mating success and Allee effects in invading gypsy moth populations. *J Anim Ecol* 77(5):966–973.
- Suarez AV, Holway DA, Case TJ (2001) Patterns of spread in biological invasions dominated by long-distance jump dispersal: Insights from Argentine ants. *Proc Natl Acad Sci USA* 98(3):1095–1100.
- Winston ML (1992) The biology and management of africanized honey bees. *Annu Rev Entomol* 37(1):173–193.
- Shigesada N, Kawasaki K (1997) *Biological Invasions: Theory and Practice* (Oxford University Press, Oxford).
- McClure MS (1990) Role of wind, birds, deer, and humans in the dispersal of hemlock woolly adelgid (Homoptera: Adelgidae). *Environ Entomol* 19(1):36–43.
- Johnston DM, Liebhold AM, Tobin PC, Bjornstad ON (2006) Allee effects and pulsed invasion by the gypsy moth. *Nature* 444(7117):361–363.
- Kauffman MJ, Jules ES (2006) Heterogeneity shapes invasion: Host size and environment influence susceptibility to a nonnative pathogen. *Ecol Appl* 16(1):166–175.
- Laine A-L, Hanski I (2006) Large-scale spatial dynamics of a specialist plant pathogen in a fragmented landscape. *J Ecol* 94(1):217–226.
- Shigesada N, Kawasaki K, Takeda Y (1995) Modeling stratified diffusion in biological invasions. *Am Nat* 146(2):229–251.
- Liebhold AM, Tobin PC (2008) Population ecology of insect invasions and their management. *Annu Rev Entomol* 53(1):387–408.
- Holt RD (1985) Population dynamics in two-patch environments: Some anomalous consequences of an optimal habitat distribution. *Theor Popul Biol* 28(2):181–208.
- Pulliam HR (1988) Sources, sinks, and population regulation. *Am Nat* 132(5):652–661.
- Greene CM (2003) Habitat selection reduces extinction of populations subject to Allee effects. *Theor Popul Biol* 64(1):1–10.
- Kaplan HB, Greenberg EP (1985) Diffusion of autoinducer is involved in regulation of the *Vibrio fischeri* luminescence system. *J Bacteriol* 163(3):1210–1214.
- Miller MB, Bassler BL (2001) Quorum sensing in bacteria. *Annu Rev Microbiol* 55(1):165–199.
- Van Melderen L, et al. (1996) ATP-dependent degradation of CcdA by Lon protease. Effects of secondary structure and heterologous subunit interactions. *J Biol Chem* 271(44):27730–27738.
- Dao-Thi MH, et al. (2005) Molecular basis of gyrase poisoning by the addition toxin CcdB. *J Mol Biol* 348(5):1091–1102.
- Vogel U, Jensen KF (1994) The RNA chain elongation rate in *Escherichia coli* depends on the growth rate. *J Bacteriol* 176(10):2807–2813.
- Dennis PP, Bremer H (1974) Differential rate of ribosomal protein synthesis in *Escherichia coli* B/r. *J Mol Biol* 84(3):407–422.
- Volkmer B, Heinemann M (2011) Condition-dependent cell volume and concentration of *Escherichia coli* to facilitate data conversion for systems biology modeling. *PLoS ONE* 6(7):e23126.
- Collins CH, Leadbetter JR, Arnold FH (2006) Dual selection enhances the signaling specificity of a variant of the quorum-sensing transcriptional activator LuxR. *Nat Biotechnol* 24(6):708–712.
- Haseltine EL, Arnold FH (2008) Implications of rewiring bacterial quorum sensing. *Appl Environ Microbiol* 74(2):437–445.
- Dwyer DJ, Kohanski MA, Hayete B, Collins JJ (2007) Gyrase inhibitors induce an oxidative damage cellular death pathway in *Escherichia coli*. *Mol Syst Biol* 3:91.

79. Canton B, Labno A, Endy D (2008) Refinement and standardization of synthetic biological parts and devices. *Nat Biotechnol* 26(7):787–793.
80. Urbanowski ML, Lostro CP, Greenberg EP (2004) Reversible acyl-homoserine lactone binding to purified *Vibrio fischeri* LuxR protein. *J Bacteriol* 186(3):631–637.
81. Liebhold A, Bascompte J (2003) The Allee effect, stochastic dynamics and the eradication of alien species. *Ecol Lett* 6(2):133–140.
82. Tien NSH, Sabelis MW, Egas M (2011) Ambulatory dispersal in *Tetranychus urticae*: An artificial selection experiment on propensity to disperse yields no response. *Exp Appl Acarol* 53(4):349–360.
83. Hanski I, Alho J, Moilanen A (2000) Estimating the parameters of survival and migration of individuals in metapopulations. *Ecology* 81(1):239–251.
84. Schtickzelle N, Mennechez G, Baguette M (2006) Dispersal depression with habitat fragmentation in the bog fritillary butterfly. *Ecology* 87(4):1057–1065.
85. Ronce O (2007) How does it feel to be like a rolling stone? Ten questions about dispersal evolution. *Annu Rev Ecol Syst* 38(1):231–253.
86. Englmann M, et al. (2007) The hydrolysis of unsubstituted N-acylhomoserine lactones to their homoserine metabolites: Analytical approaches using ultra performance liquid chromatography. *J Chromatogr A* 1160(1–2):184–193.
87. Bogdanowicz S, Wallner W, Bell J, Odell T, Harrison R (1993) Asian gypsy moths (Lepidoptera: Lymantriidae) in North America: Evidence from molecular data. *Ann Entomol Soc Am* 86(6):710–715.
88. Vercken E, Kramer AM, Tobin PC, Drake JM (2011) Critical patch size generated by Allee effect in gypsy moth, *Lymantria dispar* (L.). *Ecol Lett* 14(2):179–186.
89. Menéndez R, Gutiérrez D, Thomas CD (2002) Migration and Allee effects in the six-spot burnet moth *Zygaena filipendulae*. *Ecol Entomol* 27(3):317–325.
90. Kuussaari M, et al. (1998) Allee effect and population dynamics in the glanville fritillary butterfly. *Oikos* 82(2):384–392.
91. Dunstan P, Bax N (2007) How far can marine species go? Influence of population biology and larval movement on future range limits. *Mar Ecol Prog Ser* 344:15–28.
92. Rhainds M, Fagan WF (2010) Broad-scale latitudinal variation in female reproductive success contributes to the maintenance of a geographic range boundary in bagworms (Lepidoptera: Psychidae). *PLoS ONE* 5(11):e14166.
93. Cronin JT (2009) Movement, colonization, and establishment success of a planthopper of prairie potholes, *Delphacodes scolochloa* (Hemiptera: Delphacidae). *Ecol Entomol* 34(1):114–124.
94. Petit J, Hoddle M, Grandgirard J, Roderick G, Davies N (2008) Invasion dynamics of the glassy-winged sharpshooter (*Homalodisca vitripennis*) (Germar) (Hemiptera: Cicadellidae) in French Polynesia. *Biol Invasions* 10(7):955–967.
95. Liermann M, Hilborn R (2001) Depensation: Evidence, models and implications. *Fish Fish* 2(1):33–58.
96. Brockett BFT, Hassall M (2005) The existence of an Allee effect in populations of *Porcellio scaber* (Isopoda: Oniscidea). *Eur J Soil Biol* 41(3):123–127.
97. Wertheim B, Marchais J, Vet LEM, Dicke M (2002) Allee effect in larval resource exploitation in *Drosophila*: An interaction among density of adults, larvae, and micro-organisms. *Ecol Entomol* 27(5):608–617.
98. Sakuratani Y, Nakao K, Aoki N, Sugimoto T (2001) Effect of population density of *Cylas formicarius* (Fabricius) (Coleoptera: Brentidae) on the progeny populations. *Appl Entomol Zool* 36(1):19–23.
99. Schlyter F, Birgersson G, Byers JA, Löfqvist J, Bergström G (1987) Field response of spruce bark beetle, *Ips typographus*, to aggregation pheromone candidates. *J Chem Ecol* 13(4):701–716.
100. Donnenberg MS (2000) Pathogenic strategies of enteric bacteria. *Nature* 406(6797):768–774.
101. Rooijackers SHM, van Kessel KPM, van Strijp JAG (2005) Staphylococcal innate immune evasion. *Trends Microbiol* 13(12):596–601.
102. De Kievit TR, Gillis R, Marx S, Brown C, Iglewski BH (2001) Quorum-sensing genes in *Pseudomonas aeruginosa* biofilms: Their role and expression patterns. *Appl Environ Microbiol* 67(4):1865–1873.
103. Kadam SV, Velicer GJ (2006) Variable patterns of density-dependent survival in social bacteria. *Behav Ecol* 17(5):833–838.
104. Van Melderen L, Bernard P, Couturier M (1994) Lon-dependent proteolysis of CcdA is the key control for activation of CcdB in plasmid-free segregant bacteria. *Mol Microbiol* 11(6):1151–1157.
105. Pai A, You L (2009) Optimal tuning of bacterial sensing potential. *Mol Syst Biol* 5:286.
106. Ravn L, Christensen AB, Molin S, Givskov M, Gram L (2001) Methods for detecting acylated homoserine lactones produced by Gram-negative bacteria and their application in studies of AHL-production kinetics. *J Microbiol Methods* 44(3):239–251.
107. Kaufmann GF, et al. (2005) Revisiting quorum sensing: Discovery of additional chemical and biological functions for 3-oxo-N-acylhomoserine lactones. *Proc Natl Acad Sci USA* 102(2):309–314.
108. Koenig W, Dickinson J (2004) *Ecology and Evolution of Cooperative Breeding Birds* (Cambridge University Press, Cambridge).
109. Ridley AR (2012) Invading together: The benefits of coalition dispersal in a cooperative bird. *Behav Ecol Sociobiol* 66(1):77–83.
110. Schoof V, Rie AM, Jack KM, Isbell LA (2009) What traits promote male parallel dispersal in primates? *Behaviour* 146(4–5):701–726.
111. Branch LC, Villarreal D, Fowler GS (1993) Recruitment, dispersal, and group fusion in a declining population of the plains Vizcacha (*Lagostomus maximus*; Chinchillidae). *J Mammal* 74(1):9–20.
112. Reichling SB (2000) Group dispersal in juvenile *Brachypelma vagans* (Araneae, Theraphosidae). *J Arachnol* 28(2):248–250.
113. Heinsohn R, Dunn P, Legge S, Double M (2000) Coalitions of relatives and reproductive skew in cooperatively breeding white-winged choughs. *Proc Biol Sci* 267(1440):243–249.
114. Williams DA, Rabenold KN (2005) Male-biased dispersal, female philopatry, and routes to fitness in a social corvid. *J Anim Ecol* 74(1):150–159.
115. Pusey AE, Packer C (1987) The evolution of sex-biased dispersal in lions. *Behaviour* 101(4):275–310.
116. Doolan SP, Macdonald DW (1996) Dispersal and extra-territorial prospecting by slender-tailed meerkats (*Suricata suricatta*) in the south-western Kalahari. *J Zool* 240(1):59–73.
117. Berleman JE, et al. (2011) FrzS regulates social motility in *Myxococcus xanthus* by controlling exopolysaccharide production. *PLoS ONE* 6(8):e23920.
118. Brenner K, Arnold FH (2011) Self-organization, layered structure, and aggregation enhance persistence of a synthetic biofilm consortium. *PLoS ONE* 6(2):e16791.
119. Butler MT, Wang Q, Harshey RM (2010) Cell density and mobility protect swarming bacteria against antibiotics. *Proc Natl Acad Sci USA* 107(8):3776–3781.

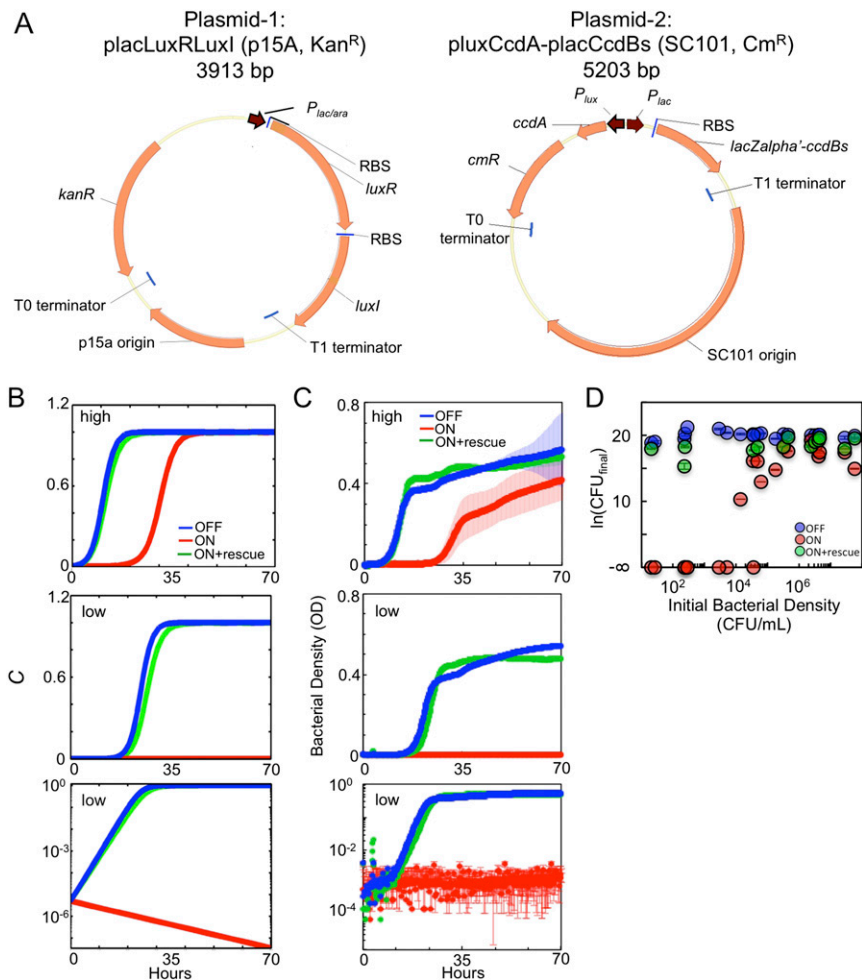


Fig. S1. Plasmids and growth curves of our engineered bacteria. (A) The circuit conferring a strong Allee effect was created in *E. coli* using two plasmids. Replication origin and antibiotic resistant marker are described in parentheses. Promoters (red arrows, where the direction of the arrow indicates orientation), ribosomal binding sequences (RBS; blue lines perpendicular to plasmid), genes (orange arrows), and terminators (blue lines parallel to plasmid) are indicated on each plasmid. Size of the plasmid [in base pairs (bp)] is indicated below the name of the plasmid. *kanR* and *cmR* confer Kan^R and Cm^R. Construction of the plasmids, including estimated copy number per cell, is described in *SI Materials and Methods*. (B) Simulated growth curves of our engineered bacteria. With the circuit OFF or ON + rescue, bacterial density (C) is predicted to increase regardless of the initial C. With the circuit ON, bacterial density increases only when the initial C is sufficiently high; otherwise, the population goes extinct. (Top) High initial $C = 5 \times 10^{-3}$. (Middle) Low initial $C = 5 \times 10^{-6}$. (Bottom) The same data as Middle but y axis is plotted on log scale. [A] (ON + rescue) = 0.1 μM . (C) Experimental growth curves of our engineered bacteria. With the circuit OFF (–IPTG) or ON + rescue (+IPTG/AHL), bacterial density increased at both low (Middle) and high (Top) initial bacterial densities. With the circuit ON (+IPTG), cultures initiated with a sufficiently high density grew, whereas those with a low initial density did not grow. High initial density was initiated from $\sim 10^8$ cfu/mL. Low initial density was initiated from $\sim 10^4$ cfu/mL. (Bottom) The same data as Middle but the y axis is plotted on a log scale. Bacteria grown in the OFF and ON + rescue conditions have similar specific growth rates ($P = 0.18$, two-tailed t test; *SI Materials and Methods*). This suggests that 0.1 μM AHL can likely lead to sufficient production of CcdA to inhibit CcdB. SD from three replicates. (D) Bistability plot of our engineered bacteria. With the circuit OFF (–IPTG) or ON + rescue (+IPTG/AHL), the number of cfus observed after 28 h was positive regardless of initial cell density. With the circuit ON (+IPTG), cfus were not detected after 28 h below an initial density of $\sim 10^4$ cfu/mL. Otherwise, the number of cfus increased. Note that these data are identical to those plotted in Fig. 1C. When $\text{cfu}_{\text{final}}$ was 0, a result of negative infinity was obtained. SD from three replicates.

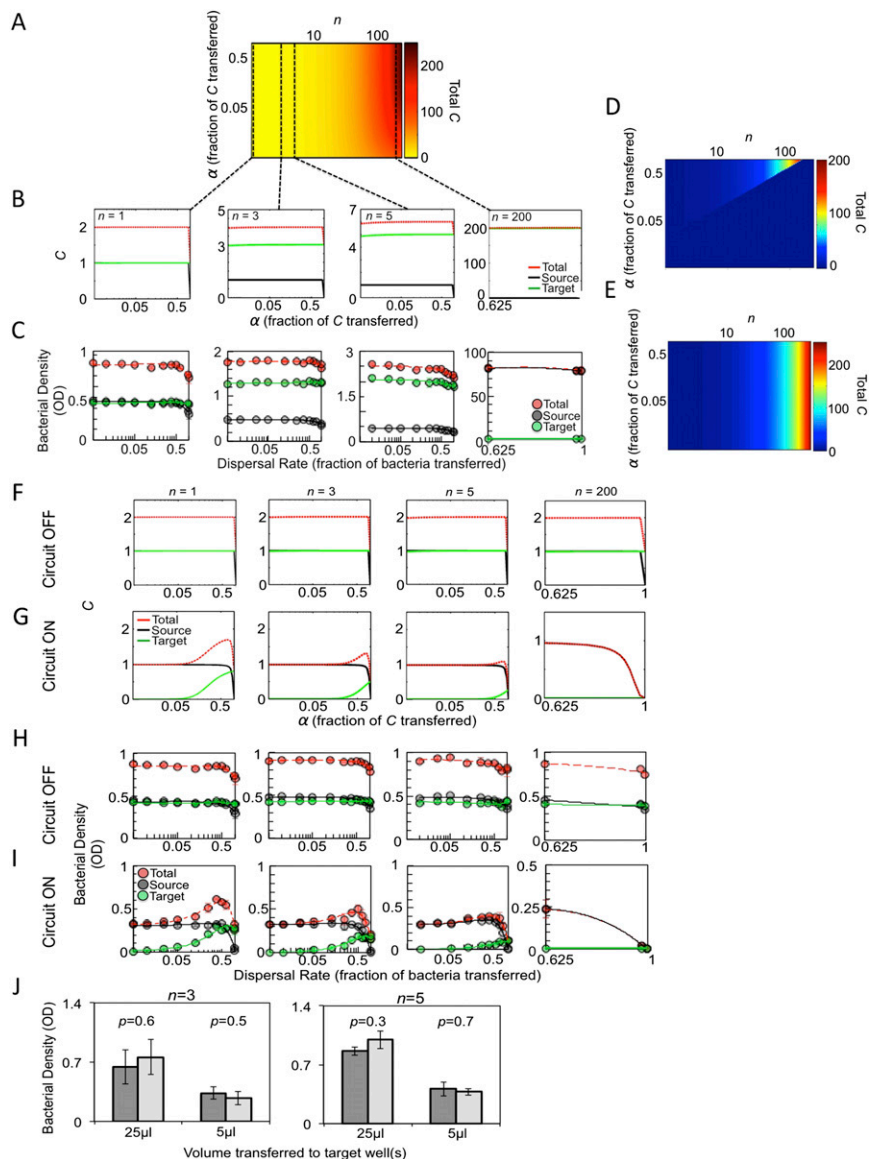


Fig. S4. Without a strong Allee effect, spread occurs regardless of dispersal rate and the number of target sites. This figure also shows raw data for multitarget patch experiments (OD for one target patch is shown). OD values shown in *H* and *I* are multiplied by the number of target patches (n) to produce the data shown in Fig. 4 and Fig. S4C (*SI Materials and Methods*). (A) Simulated spread landscape for multitarget dispersal in the absence of a strong Allee effect. With the circuit OFF, our model predicts that spread occurs regardless of n when $0 < \alpha < 1$. Initial $C = 0.05$, $t = 28$ h. (B) Slices of the spread landscape along the x axis with increasing values of n . n is indicated in each panel. (C) Density of bacterial populations with increasing dispersal rate and number of target wells. With the circuit OFF, spread occurs regardless of dispersal rate when the number of target wells was 1, 3, 5, or 200. SD from six replicates. The density of each target well was obtained by multiplying the target well by n as described in *SI Materials and Methods*. Experiments initiated from an initial density of $5.8 \pm 1.2 \times 10^6$ cfu/mL. OD was measured at 28 h. Lines drawn as a guide. (D) Simulated spread landscape at steady state. The transient increase at intermediate values of n (number of target patches) is no longer observed. However, as n increases, the range of dispersal rates (α) allowing spread continues to decrease. $t = 1,000$ h. (E) Simulated spread landscape at steady state. Spread occurs at all values of n regardless of α . $t = 1,000$ h. (F) Model predictions for multitarget patch experiments in the absence of a strong Allee effect (i.e., circuit OFF) when only one target patch (of all total patches) is considered. (G) Model predictions for multitarget patch experiments in the presence of a strong Allee effect (i.e., circuit ON) when only one target patch (of all total patches) is considered. (H) Density of bacterial populations that do not exhibit an Allee effect (circuit OFF, -IPTG) with increasing dispersal rates and increasing number of target wells. Our experimental system confirmed our modeling predictions. For all panels containing experimental data, the number of target wells is indicated in each panel. Experiments were initiated from an initial density of $5.8 \pm 1.2 \times 10^6$ cfu/mL. OD was measured at 28 h. Lines drawn as a guide (for both *C* and *D*). (I) Density of bacterial populations that exhibit a strong Allee effect (circuit ON, +IPTG) with increasing dispersal rates and increasing number of target wells. Our experimental system confirmed our modeling predictions. (J) To produce the data in Fig. 4 and in Fig. S4C, we assumed that one well could function as a surrogate of n wells. We confirmed this assumption as described in *SI Materials and Methods*. Light gray bars represent the OD from dispersal that occurred to one target well that was then multiplied by the total number of target wells [either three (*Left*) or five (*Right*)]. Dark gray bars represent the summed total OD observed when dispersal occurred to either three (*Left*) or five (*Right*) individual target wells. Final bacterial density produced using either experiment was not significantly different (as indicated in the figure, two-tailed *t* test). The volume of medium transferred from the source to the target well is represented by 25 μ L and 5 μ L. OD was measured at 28 h. SD from four replicates.

Table S2. A summary of cooperative species that have an Allee effect due to environmental conditioning

Species	Findings	Refs.
Alpine marmots (<i>Marmota marmota</i>)	Small groups had less efficient thermoregulation during hibernation.	(14)
Woodlouse (<i>Porcellio scaber</i>)	Group sheltering during periods of water loss allows water retention and increases fitness.	(96)
Monarch butterflies (<i>Danaus plexippus</i>)	Reproductive success of small over-wintering aggregates (i.e., groups of individuals) is lower than larger aggregates.	(7)
Pale-swallow wort (<i>Vincetoxicum rossicum</i>)	Secretion of allelopathic (i.e., chemical) compounds suppresses competitor plant growth. Small groups of plants had lower biomass and produced less seeds.	(8)
<i>Drosophila melanogaster</i>	Pheromone-mediated high-density aggregation of adult larvae on medium increased the reproductive success of a population by reducing the growth of competing fungi.	(97)
Sweet potato weevil (<i>Cylas formicarius</i>)	Increased mortality of eggs and larvae at low density due to a reduction in the amount of secreted chemical hampering the ability of <i>C. formicarius</i> to feed.	(98)
European spruce bark beetle (<i>Ips typographus</i>)	Release of aggregating pheromones promotes aggregating on trees, allowing beetles to overwhelm plant defenses and feed.	(13, 99)
<i>Vibrio cholera</i>	Secretion of cholera toxin, which is initiated at a sufficiently high cell density, is a limiting step during the infection process.	(100)
<i>Staphylococcus aureus</i>	Successful infection requires the secretion of several immune system modulating factors. Secretion requires a minimal density of bacteria.	(15, 18, 101)
<i>Pseudomonas aeruginosa</i>	The formation of biofilms can be regulated through quorum-sensing molecules. Such biofilms have increased antibiotic resistance.	(22, 102)
<i>Myxococcus xanthus</i>	A minimum density of cells is required to form a fruiting body structure.	(103)

Multiple additional examples can be found elsewhere (10, 15, 33, 95).

Table S3. Parameters used to estimate the magnitude of β and γ and those used in the simplified model

Parameter	Description	Rate constant	Source
Parameters used to estimate β and γ			
k_{kill}	Bacterial killing rate by CcdB	0.8 h^{-1}	(3)
k_{d1}	Degradation rate constant of CcdA	1.38 h^{-1}	(104)
k_{d2}	Degradation rate constant of CcdB	0.30 h^{-1}	(104)
k_{d3}	Degradation rate constant of CcdA–CcdB complex	0.69 h^{-1}	(71)
k_{ca}	Expression rate constant of CcdA	1 h^{-1}	Estimated
k_l	Synthesis rate constant of CcdB	$5 \times 10^{-3} \mu\text{M h}^{-1}$	Estimated
K	CcdB concentration that gives rise to the half maximal killing rate	$5 \times 10^{-2} \mu\text{M}$	Estimated
Parameters used in the simplified model			
μ	Maximum specific growth rate	0.5 h^{-1}	Estimated from Fig. S1C
k_A	Synthesis rate constant of AHL	$0.25 \mu\text{M h}^{-1}$	(105, 106)
k_{dA}	Degradation rate constant of AHL	0.01 h^{-1}	(107)
γ	Killing rate of CcdB	$4 \times 10^{-3} \mu\text{M h}^{-1}$	*
β	Half maximal killing ability of CcdB	$7 \times 10^{-3} [\mu\text{M}]$	*
τ	Time delay of the activation of gene expression by the LuxR–AHL complex	7 h	Estimated from Fig. S1C

Eqs. S10 and S11.

*These values were determined by first estimating the order of magnitude of each parameter using information in "Parameters used to estimate β and γ ." The parameter value was then fit to our experimental data from Figs. 1C and 2.

